

On inference for modularity statistics in structured networks

Anirban Mitra, Konasale Prasad, Joshua Cape*

Department of Statistics, University of Pittsburgh
Department of Psychiatry, University of Pittsburgh
Department of Statistics, University of Wisconsin–Madison

Abstract

This paper revisits the classical concept of network modularity and its spectral relaxations used throughout graph data analysis. We formulate and study several modularity statistic variants for which we establish asymptotic distributional results in the large-network limit for networks exhibiting nodal community structure. Our work facilitates testing for network differences and can be used in conjunction with existing theoretical guarantees for stochastic blockmodel random graphs. Our results are enabled by recent advances in the study of low-rank truncations of large network adjacency matrices. We provide confirmatory simulation studies and real data analysis pertaining to the network neuroscience study of psychosis, specifically schizophrenia. Collectively, this paper contributes to the limited existing literature to date on statistical inference for modularity-based network analysis. Supplemental materials for this article are available online.

Keywords: blockmodel, latent structure, modularity, network, random graph.

*The authors thank Nicholas Theis and the entire CONCEPT lab for real data expertise. This research uses data from the UK Biobank, a major biomedical database, obtained from the UK Biobank Resource under application number 68923 (PI: Konasale Prasad). This research was supported in part by the University of Pittsburgh Center for Research Computing through the resources provided. Specifically, this work used the H2P cluster which is supported by NSF award number OAC-2117681. JC gratefully acknowledges support from the University of Wisconsin–Madison, Office of the Vice Chancellor for Research and Graduate Education, with funding from the Wisconsin Alumni Research Foundation.

1 Introduction

Networks and graph-structured data, comprised of nodes (i.e., entities) and edges (i.e., pairwise interactions), are frequently analyzed in an effort to determine the extent to which nodal community structure is present. Modularity-based measures have emerged as popular criteria for quantifying the existence of nodal organization via edge connectivity patterns, commonly described as *modules*, *clusters*, or *communities* (Newman, 2018). Examples of so-called modules or groups of network nodes include friendship circles among people in social networks (Zachary, 1977, Leung et al., 2014, Fitzpatrick et al., 2018, Li et al., 2020) and ensembles of brain regions exhibiting high functional or structural connectivity in neuroimaging scans (Rubinov and Sporns, 2010, Power et al., 2011, Grayson and Fair, 2017).

Finding modules has meaningful downstream consequences for subsequent interventions and inference, for example, towards promoting diversity in social or political interactions (Eulau and Siegel, 1981, Porter et al., 2005), and towards developing precision medicine or therapies for health disorders (Capriotti et al., 2019, Tan et al., 2019). Modularity analysis has been applied in the study of mobile communication networks to suggest that linguistic ‘borders’ or ‘divides’ are influenced by a combination of geographic, political, and demographic factors (Blondel et al., 2010). Elsewhere, Guimerà et al. (2005) applies modularity maximization to detect communities in the worldwide air transportation network, finding that module structure and formation are driven by geopolitics and not simply by geographic physical proximity alone.

In practice, given a collection of observed networks, analysts often compute various graph-theoretic summary statistics, including modularity values, for the purpose of comparing and contrasting the networks. Differences between individual networks or populations of networks are then reported and interpreted, sometimes but not always accompanied by empirical, simulation-based, or model-assisted proxies for quantifying uncertainty in the reported statistics. For example, colloquially, Network A or (networks in) Population A might be reported as being ‘more modular’ (or, say, more connected, or sparser) than Network B or (networks in) Population B.

The purpose of this article is to contribute towards a deeper theoretical and methodological understanding of modularity statistics and their variability in the context of random graph models. The limited availability of statistical inference tools for modularity-based analysis has been noted

elsewhere in the literature, notably in [Ma and Barnett \(2020\)](#) which, pertinent to the present paper, establishes the asymptotic distribution of a modularity statistic for large data matrices arising from the Gaussian Orthogonal Ensemble. Other relevant works include [Li and Qi \(2020\)](#) which establishes asymptotic normality of the Newman–Girvan modularity statistic for large networks under the null hypothesis of so-called free labeling, for the purpose of testing whether a given partition has arisen completely at random. [Zhang and Chen \(2017\)](#) provides a hypothesis testing framework for assessing the significance of detected communities where the space of null models is the set of simple graphs having the same degree sequence as the observed graph. See also the highly influential asymptotic analysis carried out in [Bickel and Chen \(2009\)](#).

Here, we briefly preface the content that follows. In this paper, we focus on several well-motivated cases of a to-be-specified general modularity function, drawing on the spectral (eigen) properties of large network adjacency matrices. For regimes where ground truth community assignments are asymptotically uniformly perfectly recoverable in stochastic blockmodel random graphs, we establish the asymptotic normality of modularity values with explicit asymptotic bias and variance expressions. We provide detailed simulations to illustrate these findings and provide real data examples involving human brain networks. Further extensions and complements are also discussed.

2 Background

2.1 Random graph models

A diversity of random graph models are encountered throughout the network-focused literature in statistics, mathematics, and physics. Two extremal examples at opposite ends of the proverbial spectrum include homogeneous and inhomogeneous Erdős–Rényi graphs ([Erdős and Rényi, 1959](#), [Gilbert, 1959](#), [Bollobás et al., 2007](#)). In this paper, we compromise between simplicity and generality by focusing on stochastic blockmodel (SBM) graphs ([Holland et al., 1983](#)).

Definition 2.1 (Stochastic blockmodel random graphs). Let $K \geq 2$ be a positive integer. Let $\boldsymbol{\pi} \in \mathcal{S}_{K-1}$ be a non-negative vector in the interior of the $(K - 1)$ -dimensional simplex in \mathbb{R}^K , whence $0 < \pi_k < 1$ for each $1 \leq k \leq K$ with $\sum_{k=1}^K \pi_k = 1$. Let $\mathbf{B} \in (0, 1)^{K \times K}$ be a symmetric matrix of probabilities. First, sample i.i.d. categorical random variables τ_1, \dots, τ_n according to

$\mathbb{P}[\tau_i = k] = \pi_k$ to form the membership vector $\boldsymbol{\tau} = (\tau_1, \dots, \tau_n)^\top$. Second, conditional on $\boldsymbol{\tau}$, generate a binary symmetric random adjacency matrix $\mathbf{A} \in \{0, 1\}^{n \times n}$ according to $A_{ij} \sim \text{Bernoulli}(\rho_n B_{\tau_i \tau_j})$ independently for all $i \leq j$, where $\rho_n \in (0, 1]$ denotes a sparsity factor. We then write $(\mathbf{A}, \boldsymbol{\tau}) \sim \text{SBM}(\mathbf{B}, \boldsymbol{\pi})$ with accompanying sparsity factor ρ_n . We write $\mathbf{A} \sim \text{SBM}(\mathbf{B}, \boldsymbol{\pi})$ with sparsity factor ρ_n when only \mathbf{A} is observed, i.e., when $\boldsymbol{\tau}$ is integrated out from $(\mathbf{A}, \boldsymbol{\tau})$.

Stochastic blockmodeling provides a useful framework for modeling nodal clustering and connectivity. The block structure in SBMs corresponds to the concept of nodal communities. Further, SBMs need not place any additional restrictions *a priori* on the within-block versus between-block edge connectivity probabilities. For example, letting $\mathbb{I}_{\{\cdot\}}$ denote the binary indicator function, an SBM graph with edge probabilities given by $B_{\tau_i \tau_j} = a \cdot \mathbb{I}_{\{\tau_i = \tau_j\}} + b \cdot \mathbb{I}_{\{\tau_i \neq \tau_j\}}$ for all $1 \leq \tau_i, \tau_j \leq K$ exhibits assortativity (i.e., homophily) when $a > b$ but is disassortative (i.e., heterophilic) when $a < b$. Beyond homogeneous assortativity and disassortativity, more complex connectivity phenomena are enabled by the at most $K(K+1)/2$ distinct entries of \mathbf{B} , such as core-periphery network structure.

Stochastic blockmodels have received considerable research attention in recent years (Abbe, 2018, Lee and Wilkinson, 2019). As such, they produce random graphs whose statistical properties are increasingly better and better understood. While outside the scope of the present paper, popular SBM variants include degree-corrected SBMs (Karrer and Newman, 2011) which permit node-specific degree heterogeneity, mixed-membership SBMs (Airoldi et al., 2008) which permit node-specific weighted multi-block memberships, weighted SBMs (Aicher et al., 2013, 2014) which permit heterogeneous edge weights, popularity-adjusted SBMs (Sengupta and Chen, 2018, Koo et al., 2023), and covariate-adjusted SBMs (Sweet, 2015, Zhang et al., 2019).

2.2 Basics of network modularity

Let $\mathbf{A} = (A_{ij}) \in \mathbb{R}^{n \times n}$ denote a (possibly weighted) adjacency matrix corresponding to an undirected n -node graph \mathcal{G} . Given a posited ‘null network’ $\mathbf{P} = (P_{ij}) \in \mathbb{R}^{n \times n}$ serving as a benchmark for \mathbf{A} , and given a partition of $\llbracket n \rrbracket := \{1, 2, \dots, n\}$ encoded by the cluster membership vector $\boldsymbol{\tau}$, a general formulation of the modularity quality function (Bazzi et al., 2016) is given by

$$Q \equiv Q(\boldsymbol{\tau}; \mathbf{A}, \mathbf{P}) := \sum_{1 \leq i, j \leq n} (A_{ij} - P_{ij}) \mathbb{I}_{\{\tau_i = \tau_j\}}. \quad (1)$$

In words, Q reflects the partition-specific discrepancy between the total edge weights in the observed network and the total anticipated edge weights in the referential, posited null network. Large values of Q provide partition-specific evidence vis-à-vis τ that the observed network is more modular than by chance alone. Evaluating this discrepancy across numerous partitions $\tau \in \mathcal{T}$, or attempts at all possible partitions, naturally leads to the modularity maximization problem

$$(\arg) \max_{\tau \in \mathcal{T}} Q(\tau; \mathbf{A}, \mathbf{P}) \quad (2)$$

and computational schemes for solving relaxations thereof. The use of parentheses in Eq. (2) indicates interest both in the maximizing partition and the maximum modularity value.

For undirected unweighted graphs \mathcal{G} , historically the most commonly adopted choice of modularity function is due to Newman and Girvan, denoted by Q_{NG} , with the specification $P_{ij} = k_i k_j / (2m)$, where $k_i = \sum_{j=1}^n A_{ij}$ denotes the degree of node i in \mathbf{A} , and $m = \sum_{i=1}^n k_i / 2$ denotes the total number of graph edges (Newman and Girvan, 2004). Further dividing Q_{NG} by $2m$ yields normalized modularity values in a bounded interval. The choice Q_{NG} has the attractive property of specifying a data-dependent benchmark yet is not assumption-free, for it takes the configuration model as the underlying null model for observable random graphs (Newman, 2018).

To date, numerous algorithms and optimization procedures have been proposed for Eq. (2) and specifically for discovering community structure using Q_{NG} . Agglomerative algorithms for modularity maximization include Newman (2004), with Clauset et al. (2004) adopting a fast greedy approach, and Blondel et al. (2008) proposing the Louvain heuristic. Brandes et al. (2008) provides an integer linear programming approach for modularity maximization. Traag et al. (2019) suggests the Leiden algorithm as an improvement over the Louvain algorithm by allowing for and “aggregating over refined partitioning of the communities” during the stage of “local moving of nodes.” Other methods for optimizing modularity include extremal optimization (Duch and Arenas, 2005) and simulated annealing (Reichardt and Bornholdt, 2006).

Yet another popular approach for modularity maximization is to consider spectral relaxations via the eigendecomposition of the modularity matrix (Newman, 2006b). In the case of two communities, defining the membership vector as having entries either $+1$ or -1 permits rewriting Q_{NG} as a scaled quadratic form. The element-wise choice of sign is derived from the component-wise

signs of the eigenvector corresponding to the largest positive eigenvalue of the modularity matrix. To generalize the method for detecting more than two communities, successive bipartitioning can be applied. Newman (2006a) adopts an alternative approach for $K > 2$ by considering an $n \times K$ matrix whose one-hot-encoded columns represent node-community correspondences.

We mention in passing that modularity considerations for graphons have recently been investigated in Klimm et al. (2022), defined akin to Newman–Girvan modularity but with a modularity surface in place of a modularity matrix. The study of multi-layer networks has also recently garnered attention (Dong et al., 2012, Lei et al., 2019, Bhattacharyya and Chatterjee, 2020) thereby motivating further extensions of modularity functions and modularity maximization concepts (Mucha et al., 2010, Bazzi et al., 2016, De Domenico et al., 2015a,b, De Domenico, 2017).

3 Modularity-based inference

3.1 Modularity variants

As mentioned above, a common approach to modularity maximization and analysis is to resort to spectral relaxations of Eq. (2), which, in the language of this paper, leads to computing eigenvalues and eigenvectors associated to the matrix $\mathbf{A} - \mathbf{P}$. We adopt a related but slightly different approach, motivated by several key observations in Tang et al. (2022) and related works. The first observation is that so-called strong consistency of eigenvector-based clustering holds for not-too-sparse stochastic blockmodel graphs (Xie, 2022, Rubin-Delanchy et al., 2022, Lyzinski et al., 2014). In particular, for such SBMs, $\hat{\boldsymbol{\tau}}$ derived from the leading eigenvectors of \mathbf{A} perfectly and uniformly recovers the unobserved true memberships encoded in $\boldsymbol{\tau}$ in ℓ_∞ vector norm with probability rapidly tending to one in the large-network limit. The second key observation is that computing truncated eigendecompositions of large data matrices exhibiting approximately low-rank population-level structure has the effect of data denoising. Quantitatively, a suitable low-rank truncation of \mathbf{A} , denoted by $\hat{\mathbf{A}}$, yields a better approximation to $\mathbb{E}[\mathbf{A} \mid \boldsymbol{\tau}]$ than does \mathbf{A} itself. Taken together, we are led to formulate and study the following three modularity statistics.

Definition 3.1 (Likelihood-based, Spectral-based and Residual-based modularities).

Denote the full eigendecomposition of the $n \times n$ symmetric matrix \mathbf{A} by $\mathbf{A} = \sum_{i=1}^n \hat{\lambda}_i \hat{\mathbf{u}}_i \hat{\mathbf{u}}_i^\top$ with

eigenvalues $|\hat{\lambda}_1| \geq \dots \geq |\hat{\lambda}_n|$ and orthonormal eigenvectors $\hat{\mathbf{u}}_1, \dots, \hat{\mathbf{u}}_n \in \mathbb{R}^n$. We write $\hat{\mathbf{A}} = \sum_{i=1}^d \hat{\lambda}_i \hat{\mathbf{u}}_i \hat{\mathbf{u}}_i^\top$ to denote the top rank d approximation of \mathbf{A} . In what follows, the value d corresponds to an underlying population-level quantity (matrix rank) that is consistently estimable using \mathbf{A} and will be subsequently discussed in greater detail. Given a specified cluster membership vector $\boldsymbol{\tau}$, we consider the following three modularity variants.

$$Q_L := \sum_{i,j=1}^n (A_{ij} - P_{ij}) \mathbb{I}_{\{\tau_i=\tau_j\}}, \quad (3a)$$

$$Q_S := \sum_{i,j=1}^n (\hat{A}_{ij} - P_{ij}) \mathbb{I}_{\{\tau_i=\tau_j\}}, \quad (3b)$$

$$Q_R := \sum_{i,j=1}^n (A_{ij} - \hat{A}_{ij}) \mathbb{I}_{\{\tau_i=\tau_j\}}. \quad (3c)$$

In Definition 3.1, Q_L signifies a so-called likelihood variant of modularity in which entrywise $\mathbb{E}[A_{ij} \mid \boldsymbol{\tau}] = P_{ij}$. In words, for Q_L the benchmark null network corresponds to the expected graph adjacency matrix under the SBM generative model.

In Definition 3.1, Q_S signifies a so-called spectral variant. This choice is motivated by the fact that for not-too-sparse SBMs, $\|\hat{\mathbf{A}} - \mathbf{P}\|_{\max} \rightarrow 0$ in probability as $n \rightarrow \infty$ when d is fixed, whereas $\|\mathbf{A} - \mathbf{P}\|_{\max}$ is bounded away from zero with probability one [Tang et al. \(2022\)](#). Thus, the truncated adjacency matrix $\hat{\mathbf{A}}$ takes the place of the raw observable data \mathbf{A} , while the benchmark null network \mathbf{P} corresponding to the expected graph adjacency matrix is the same as in Q_L .

In Definition 3.1, Q_R signifies the residual or difference between the spectral and likelihood variants, i.e., $Q_R = Q_S - Q_L$. This choice is purely data-dependent, as with the Newman–Girvan formulation. Here, the raw data matrix \mathbf{A} is compared to its denoised counterpart, where these respective choices are themselves inspired by the existing literature on SBMs. This variant is further motivated by the signal-plus-noise interpretation of observed SBM adjacency matrices when written as $\mathbf{A} = \mathbf{P} + (\mathbf{A} - \mathbf{P}) = \text{signal} + \text{noise}$. Since $\hat{\mathbf{A}}$ is a spectral matrix-valued estimator of \mathbf{P} , Q_R juxtaposes within-community observed edges against denoised estimated signal in the edges.

3.2 Modularity asymptotics

3.2.1 Notational setup

Denote the Hadamard and Kronecker products for given matrices by \circ and \otimes , respectively. The vectorization of an $m \times n$ dimensional matrix \mathbf{M} is obtained by stacking its columns to yield a vector in \mathbb{R}^{mn} , denoted by $\text{vec}(\mathbf{M})$. When \mathbf{M} is symmetric, the half-vectorization is obtained by vectorizing only the lower triangular entries, including the diagonal, and is denoted by $\text{vech}(\mathbf{M})$.

Denote the (skinny) spectral decomposition of \mathbf{B} by $\mathbf{V}\boldsymbol{\Sigma}\mathbf{V}^\top$, where \mathbf{V} is a matrix of orthonormal eigenvectors and $\boldsymbol{\Sigma}$ is the diagonal matrix of non-zero eigenvalues. Letting $\boldsymbol{\nu} := \mathbf{V}|\boldsymbol{\Sigma}|^{1/2}$ yields the equivalent formulation $\mathbf{B} = \boldsymbol{\nu}\mathbf{I}_{p,q}\boldsymbol{\nu}^\top$, where $\mathbf{I}_{p,q}$ is the diagonal matrix with p diagonal entries equal to 1 and the remaining q entries equal to -1 , with $d := \text{rank}(\mathbf{B}) = p + q$. In particular, p and q reflect the number of positive and negative eigenvalues of \mathbf{B} , respectively. Define the $d \times d$ invertible matrix $\boldsymbol{\Delta} := \boldsymbol{\nu}^\top \text{diag}(\boldsymbol{\pi})\boldsymbol{\nu}$ and the idempotent matrix $\tilde{\boldsymbol{\Pi}}_{\mathbf{V}}^\perp := \mathbf{I} - \mathbf{V}(\mathbf{V}^\top \text{diag}(\boldsymbol{\pi})\mathbf{V})^{-1}\mathbf{V}^\top \text{diag}(\boldsymbol{\pi})$. Define the vector $\tilde{\boldsymbol{\pi}} = \text{vech}(\text{diag}[\pi_1^2, \dots, \pi_K^2])$ where $\text{diag}([\pi_1^2, \dots, \pi_K^2])$ is the diagonal matrix whose i -th diagonal entry is given by π_i^2 . We write \mathbf{J} to denote the matrix of all ones whose dimensionality is specified from context.

3.2.2 Asymptotic distributions for modularity statistics

The main theoretical results in this article are presented below in the form of three theorems. Each theorem is stated in terms of population-level quantities for stochastic blockmodels, namely the number of communities K , the dimension $d = \text{rank}(\mathbf{B})$, and the membership vector $\boldsymbol{\tau}$. The stated results continue to hold for appropriate estimates thereof, as discussed further below.

Theorem 3.1 (Limiting distribution for likelihood-based modularity). *For $n \geq 1$, let $\mathbf{A}^{(n)} \sim \text{SBM}(\mathbf{B}, \boldsymbol{\pi})$ be a sequence of stochastic blockmodel graphs with sparsity factor ρ_n satisfying $n\rho_n = \omega(\log n)$. Then, as $n \rightarrow \infty$, the likelihood variant of modularity in Eq. (3a) satisfies*

$$\rho_n^{-1/2} n^{-1} Q_L \xrightarrow{d} \mathcal{N}(0, \tilde{\boldsymbol{\pi}}^\top \mathbf{D}^{-1} \tilde{\boldsymbol{\pi}}). \quad (4)$$

The matrix \mathbf{D} is specified in Eq. (5) and depends on whether $\rho_n \equiv 1$ or $\rho_n \rightarrow 0$.

The matrix \mathbf{D} is the $\binom{K+1}{2} \times \binom{K+1}{2}$ diagonal matrix defined entrywise as

$$D_{(k,l),(k,l)} = \begin{cases} \frac{\pi_k \pi_l}{B_{kl}(1-B_{kl})(1+\mathbb{I}_{\{k=l\}})} & \text{if } \rho_n \equiv 1, \\ \frac{\pi_k \pi_l}{B_{kl}(1+\mathbb{I}_{\{k=l\}})} & \text{if } \rho_n \rightarrow 0. \end{cases} \quad (5)$$

Above, slight abuse of notation regarding the indices of \mathbf{D} is made for convenience. Namely, without loss of generality, we use the lower-triangular tuples $(1, 1), (2, 1), (2, 2), \dots, (K, K-1), (K, K)$ to identify the entry labels $1, 2, \dots, \binom{K+1}{2}$, in an effort to clarify the correspondence with $\text{vech}(\mathbf{B})$. By convention, entry (l, k) equals entry (k, l) .

Observe that the diagonal entries of \mathbf{D} are comparatively smaller in the sparse regime, $\rho_n \rightarrow 0$, hence the diagonal entries of \mathbf{D}^{-1} are larger, resulting in a comparatively larger asymptotic variance. The interpretation here is that sparse graphs, with their fewer observable edges and hence less available data, yield in aggregate larger variability.

Theorem 3.2 (Limiting distribution for spectral-based modularity). *For $n \geq 1$, let $\mathbf{A}^{(n)} \sim \text{SBM}(\mathbf{B}, \boldsymbol{\pi})$ be a sequence of stochastic blockmodel graphs with sparsity factor ρ_n satisfying $n\rho_n = \omega(\sqrt{n})$. Then, as $n \rightarrow \infty$, the spectral variant of modularity in Eq. (3b) satisfies*

$$\rho_n^{-1/2} n^{-1} Q_S - \rho_n^{-1/2} \tilde{\boldsymbol{\pi}}^\top \text{vech}(\boldsymbol{\Theta}) \xrightarrow{d} \mathcal{N}(0, \tilde{\boldsymbol{\pi}}^\top \tilde{\boldsymbol{\Gamma}} \tilde{\boldsymbol{\pi}}). \quad (6)$$

The matrices $\boldsymbol{\Theta}$ and $\tilde{\boldsymbol{\Gamma}}$ are specified in Eq. (7) and Eq. (8), respectively, with each depending on whether $\rho_n \equiv 1$ or $\rho_n \rightarrow 0$.

In the preceding theorem, the population-level bias and covariance terms are given by

$$\begin{aligned}
\Theta &:= \text{diag}[(\mathbf{B} \circ (\mathbf{J} - \mathbf{B}))\boldsymbol{\pi}] \boldsymbol{\nu} \boldsymbol{\Delta}^{-1} \mathbf{I}_{p,q} \boldsymbol{\Delta}^{-1} \boldsymbol{\nu}^\top \\
&\quad + \boldsymbol{\nu} \boldsymbol{\Delta}^{-1} \mathbf{I}_{p,q} \boldsymbol{\Delta}^{-1} \boldsymbol{\nu}^\top \text{diag}[(\mathbf{B} \circ (\mathbf{J} - \mathbf{B}))\boldsymbol{\pi}] \\
&\quad - \boldsymbol{\nu} \boldsymbol{\Delta}^{-1} \boldsymbol{\nu}^\top \text{diag}(\boldsymbol{\pi}) \text{diag}[(\mathbf{B} \circ (\mathbf{J} - \mathbf{B}))\boldsymbol{\pi}] \boldsymbol{\nu} \boldsymbol{\Delta}^{-1} \mathbf{I}_{p,q} \boldsymbol{\Delta}^{-1} \boldsymbol{\nu}^\top \\
&\quad - \boldsymbol{\nu} \boldsymbol{\Delta}^{-1} \mathbf{I}_{p,q} \boldsymbol{\Delta}^{-1} \boldsymbol{\nu}^\top \text{diag}[(\mathbf{B} \circ (\mathbf{J} - \mathbf{B}))\boldsymbol{\pi}] \text{diag}(\boldsymbol{\pi}) \boldsymbol{\nu} \boldsymbol{\Delta}^{-1} \boldsymbol{\nu}^\top \quad \text{if } \rho_n \equiv 1, \\
\Theta &:= \text{diag}[\mathbf{B}\boldsymbol{\pi}] \boldsymbol{\nu} \boldsymbol{\Delta}^{-1} \mathbf{I}_{p,q} \boldsymbol{\Delta}^{-1} \boldsymbol{\nu}^\top \\
&\quad + \boldsymbol{\nu} \boldsymbol{\Delta}^{-1} \mathbf{I}_{p,q} \boldsymbol{\Delta}^{-1} \boldsymbol{\nu}^\top \text{diag}[\mathbf{B}\boldsymbol{\pi}] \\
&\quad - \boldsymbol{\nu} \boldsymbol{\Delta}^{-1} \boldsymbol{\nu}^\top \text{diag}(\boldsymbol{\pi}) \text{diag}[\mathbf{B}\boldsymbol{\pi}] \boldsymbol{\nu} \boldsymbol{\Delta}^{-1} \mathbf{I}_{p,q} \boldsymbol{\Delta}^{-1} \boldsymbol{\nu}^\top \\
&\quad - \boldsymbol{\nu} \boldsymbol{\Delta}^{-1} \mathbf{I}_{p,q} \boldsymbol{\Delta}^{-1} \boldsymbol{\nu}^\top \text{diag}[\mathbf{B}\boldsymbol{\pi}] \text{diag}(\boldsymbol{\pi}) \boldsymbol{\nu} \boldsymbol{\Delta}^{-1} \boldsymbol{\nu}^\top \quad \text{if } \rho_n \rightarrow 0, \quad (7)
\end{aligned}$$

and

$$\tilde{\Gamma} := \mathcal{L}_K (\mathbf{I} - \tilde{\Pi}_V^\perp \otimes \tilde{\Pi}_V^\perp) \mathcal{D}_K \mathbf{D}^{-1} \mathcal{D}_K^\top (\mathbf{I} - \tilde{\Pi}_V^\perp \otimes \tilde{\Pi}_V^\perp)^\top \mathcal{L}_K^\top. \quad (8)$$

In Eq. (8), \mathcal{L}_K and \mathcal{D}_K denote the *elimination matrix* and *duplication matrix*, respectively (Magnus and Neudecker, 1980). For any $n \times n$ symmetric matrix \mathbf{M} , here \mathcal{L}_K is the unique $n(n+1)/2 \times n^2$ matrix satisfying $\text{vech}(\mathbf{M}) = \mathcal{L}_K \text{vec}(\mathbf{M})$. Conversely, \mathcal{D}_K is the unique $n^2 \times n(n+1)/2$ matrix satisfying $\text{vec}(\mathbf{M}) = \mathcal{D}_K \text{vech}(\mathbf{M})$.

Theorem 3.3 (Limiting distribution for residual-based modularity). *For $n \geq 1$, let $\mathbf{A}^{(n)} \sim \text{SBM}(\mathbf{B}, \boldsymbol{\pi})$ be a sequence of stochastic blockmodel graphs with sparsity factor ρ_n satisfying $n\rho_n = \omega(\sqrt{n})$. Further assume that \mathbf{B} is strictly rank-deficient, namely $d < K$. Then, as $n \rightarrow \infty$, the residual variant of modularity in Eq. (3c) satisfies*

$$\rho_n^{-1/2} n^{-1} Q_R + \rho_n^{-1/2} \tilde{\boldsymbol{\pi}}^\top \text{vech}(\Theta) \xrightarrow{d} \mathcal{N}(0, \tilde{\boldsymbol{\pi}}^\top \Gamma \tilde{\boldsymbol{\pi}}). \quad (9)$$

The matrices Θ and Γ are specified in Eq. (7) and Eq. (10), respectively, with each depending on whether $\rho_n \equiv 1$ or $\rho_n \rightarrow 0$.

In Theorem 3.3, the asymptotic covariance term Γ is given by

$$\Gamma := \mathcal{L}_K (\tilde{\Pi}_V^\perp \otimes \tilde{\Pi}_V^\perp) \mathcal{D}_K \mathbf{D}^{-1} \mathcal{D}_K^\top (\tilde{\Pi}_V^\perp \otimes \tilde{\Pi}_V^\perp)^\top \mathcal{L}_K^\top. \quad (10)$$

Theorems 3.1 to 3.3 are stated for Definition 3.1 in terms of an implicit sequence of vectors $\boldsymbol{\tau}$,

namely the ground truth SBM membership assignments. The theorem statements continue to hold for the estimated membership vector $\widehat{\boldsymbol{\tau}}$ derived from clustering the rows of the top d eigenvectors $\widehat{\mathbf{U}} \in \mathbb{R}^{n \times d}$ of \mathbf{A} appearing in $\widehat{\mathbf{A}} \equiv \widehat{\mathbf{U}}\widehat{\boldsymbol{\Lambda}}\widehat{\mathbf{U}}^\top$, due to the asymptotic perfect recovery $\widehat{\boldsymbol{\tau}} = \boldsymbol{\tau}$ as discussed in Tang et al. (2022). Furthermore, the true rank or dimension d is provably consistently estimable by an eigenvalue ratio test \widehat{d} , since for large n with high probability, $|\widehat{\lambda}_d|$ grows at the order $n\rho_n$, whereas $|\widehat{\lambda}_{d+1}|$ grows no faster than order $\sqrt{n\rho_n}$, i.e., $|\widehat{\lambda}_{d+1}| = O_{\mathbb{P}}(\sqrt{n\rho_n})$. For related discussion, see for example Rubin-Delanchy et al. (2022), Xie (2022).

In order to obtain the asymptotic normality results presented above, we decompose the modularity variants into entrywise estimators for \mathbf{B} , given below in Definition 3.2, whose distributional properties can be precisely analyzed and aggregated. Further details are given in the supplement and rely on the following definition.

Definition 3.2 (Maximum likelihood estimator and spectral estimator). For each $1 \leq k \leq K$, let n_k denote the number of nodes in community k , and define the block-specific membership vector $\mathbf{s}_k \in \{0, 1\}^n$ such that its i -th entry is 1 if $\tau_i = k$ and 0 otherwise. Let \widehat{n}_k and $\widehat{\mathbf{s}}_k$ denote estimators of n_k and \mathbf{s}_k obtained from $\widehat{\boldsymbol{\tau}}$, derived by clustering the rows of $\widehat{\mathbf{U}}$, for example using K -means clustering or an expectation–maximization algorithm for fitting a mixture of K Gaussians.

Take $\widehat{\mathbf{A}}$ to have rank $d = \text{rank}(\mathbf{B})$. For each block probability parameter B_{kl} , define the likelihood-based estimator by $\widehat{B}_{kl}^{(L)} := \frac{1}{\widehat{n}_k \widehat{n}_l \rho_n} \widehat{\mathbf{s}}_k^\top \widehat{\mathbf{A}} \widehat{\mathbf{s}}_l$. Similarly, define the spectral-based estimator by $\widehat{B}_{kl}^{(S)} := \frac{1}{\widehat{n}_k \widehat{n}_l \rho_n} \widehat{\mathbf{s}}_k^\top \widehat{\boldsymbol{\Lambda}} \widehat{\mathbf{s}}_l$. The corresponding matrix-valued estimators of \mathbf{B} are consequently denoted by $\widehat{\mathbf{B}}^{(L)}$ and $\widehat{\mathbf{B}}^{(S)}$, respectively.

We pause to remark that Theorem 3.1 requires the sparsity condition $n\rho_n = \omega(\log n)$, namely $(n\rho_n)/(\log n) \rightarrow \infty$, whereas Theorems 3.2 and 3.3 require the stronger condition $n\rho_n = \omega(\sqrt{n})$. Loosely speaking, the latter requirement arises due to a spectral bias-variance trade-off stemming from the underlying aggregation of spectral estimates; see Tang et al. (2022) for more detailed discussion and an example suggesting the potential necessity of this condition.

3.3 Hypothesis testing

The modularity variants can be used for inference by leveraging the above theorems. Supposing $\mathbf{A} \sim \text{SBM}(\mathbf{B}, \boldsymbol{\pi})$ with sparsity factor ρ_n , one may wish to test hypotheses of the form

$H_0 : \mathbf{B} = \mathbf{B}^{(0)}$, given the modular structure inherited by $(\boldsymbol{\tau}, \boldsymbol{\pi})$,

against

$H_1 : \mathbf{B} \neq \mathbf{B}^{(0)}$, given the modular structure inherited by $(\boldsymbol{\tau}, \boldsymbol{\pi})$.

For simplicity, consider the simple alternative hypothesis with connectivity matrix $\mathbf{B}^{(1)}$. For each $i = 0, 1$, under hypothesis H_i , write $\boldsymbol{\Theta}^{(i)}$ corresponding to $\boldsymbol{\Theta}$ and $\text{Var}_L^{(i)}$, $\text{Var}_S^{(i)}$ corresponding to the respective variances in Theorems 3.1 and 3.2. Upon centering Q_L and Q_S with respect to $\mathbf{B}^{(0)}$, define test statistics as follows.

1. $T_L = \frac{\rho_n^{-1/2} n^{-1} Q_L}{\sqrt{\text{Var}_L^{(0)}}}$;
2. $T_S = \frac{\rho_n^{-1/2} n^{-1} Q_S - \rho_n^{-1/2} \tilde{\boldsymbol{\pi}}^\top \text{vech } \boldsymbol{\Theta}^{(0)}}{\sqrt{\text{Var}_S^{(0)}}}$.

Let z_α be the upper- α quantile of the standard normal distribution and $\Phi(\cdot)$ denote the standard normal cumulative distribution function. For two-sided testing with the aforementioned hypotheses, the (approximate) power functions are given as follows. For the likelihood-based variant,

$$\mathbb{P}_{H_1} (|T_L| > z_{\alpha/2}) = 1 - \Phi(\mu_L + \sigma_L z_{\alpha/2}) + \Phi(\mu_L - \sigma_L z_{\alpha/2}), \quad (11)$$

where, $\sigma_L = \sqrt{\frac{\text{Var}_L^{(0)}}{\text{Var}_L^{(1)}}$ and $\mu_L = \frac{n \rho_n^{1/2} \sum_{k=1}^K \pi_k^2 (B_{kk}^{(0)} - B_{kk}^{(1)})}{\sqrt{\text{Var}_L^{(1)}}$. Similarly, for the spectral-based variant,

$$\mathbb{P}_{H_1} (|T_S| > z_{\alpha/2}) = 1 - \Phi(\mu_S + \sigma_S z_{\alpha/2}) + \Phi(\mu_S - \sigma_S z_{\alpha/2}), \quad (12)$$

where, $\sigma_S = \sqrt{\frac{\text{Var}_S^{(0)}}{\text{Var}_S^{(1)}}$ and $\mu_S = \frac{n \rho_n^{1/2} \sum_{k=1}^K \pi_k^2 (B_{kk}^{(0)} - B_{kk}^{(1)}) + \rho_n^{-1/2} \tilde{\boldsymbol{\pi}}^\top \text{vech}(\boldsymbol{\Theta}^{(0)} - \boldsymbol{\Theta}^{(1)})}{\sqrt{\text{Var}_S^{(1)}}$.

Here, testing is dictated by the diagonal elements of the block probability matrix in conjunction with the probabilities of community assignment. For example, suppose $\mathbf{B}^{(0)}$ and $\mathbf{B}^{(1)}$ are 2×2 matrices and that they differ with respect to the (1,1) diagonal element but not with respect to the (2,2) diagonal element. Instead of testing $H_0 : B_{11} = B_{11}^{(0)}$ and $B_{22} = B_{22}^{(0)}$ versus $H_1 : B_{11} = B_{11}^{(1)}$ and $B_{22} = B_{22}^{(1)}$, we take into account the relative weighing effect of π_1^2 and π_2^2 . Depending on whether π_1 is small or large, the power of the tests will range from low to high. Consequently, testing based on T_L and T_S reflects the modular structure present in \mathbf{A} .

Of note, Corollary 4 in [Tang et al. \(2022\)](#) establishes consistent estimators for terms comprising the asymptotic bias in Q_S . Additionally, one-step updates of estimators for \mathbf{B} and their asymptotic efficiency properties are studied in [Tang et al. \(2022\)](#), [Xie and Xu \(2023\)](#).

4 Simulations

We provide simulation examples illustrating the asymptotic theory developed for the modularity variants $\rho_n^{-1/2}n^{-1}Q_L$, $\rho_n^{-1/2}n^{-1}Q_S$, and $\rho_n^{-1/2}n^{-1}Q_R$ in Theorems 3.1 to 3.3. For each of the following examples, we also discuss the performance of the Louvain algorithm for clustering, a choice motivated by its historical success in the community detection problem.

4.0.1 Example 1: graphs with $K = 3$, $d = 3$, balanced, assortative

First, we consider a three-block SBM with block-probability matrix having affinity structure. We simulate 1000 independent replicates for each value n in the setting

$$\mathbf{B} = \begin{bmatrix} 0.85 & 0.50 & 0.25 \\ 0.50 & 0.85 & 0.50 \\ 0.25 & 0.50 & 0.85 \end{bmatrix}, \quad \boldsymbol{\pi} = \begin{bmatrix} 1/3 \\ 1/3 \\ 1/3 \end{bmatrix}, \quad n \in \{300, 600, 1800, 6000\}. \quad (13)$$

We present the dense case, $\rho_n \equiv 1$, as well as a sparse regime, $\rho_n = n^{-1/4}$. In both the dense and sparse regimes, the theoretical asymptotic bias is zero. For the dense regime, relatively small networks already exhibit approximate normality in simulations. When $n = 300$ (see Fig. 1), expected block sizes are 100, and the theoretical variances and bias are already well illustrated by the 1000 replicates; bias and variance estimates for different network sizes are shown in Table 1. The Louvain algorithm, which uses $Q_{\text{NG}}/2m$ as the modularity function, accurately recovers the communities with adjusted Rand index (ARI) ([Hubert and Arabie, 1985](#)) near one. The latter observation is unsurprising given the assortative (homophilic) network structure present here.

Results for the sparse regime are illustrated in Fig. 2. For the spectral variant, $n = 6000$ still corresponds to a small effective node sample size, resulting in the persistence of noticeable discrepancy between simulation and theory. For simulations with larger values of n , say $n \in \{9000, 12000\}$, the

n	$\rho_n^{-1/2} n^{-1} Q_L$				$\rho_n^{-1/2} n^{-1} Q_S$			
	Bias		Variance		Bias		Variance	
	Theory	Simulation	Theory	Simulation	Theory	Simulation	Theory	Simulation
300	0	-0.0038	0.085	0.0866	0	-0.0690	0.085	0.0887
600	0	0.0122	0.085	0.0865	0	-0.0216	0.085	0.0867
1800	0	0.0052	0.085	0.0845	0	-0.0061	0.085	0.0845
6000	0	0.0000	0.085	0.0880	0	-0.0034	0.085	0.0880

Table 1: Bias and variance for dense case in Section 4.0.1. Four decimal places are shown.

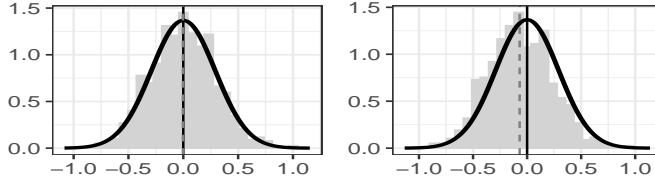


Figure 1: Dense networks in Section 4.0.1 with $n = 300$ nodes. Left plot shows $\rho_n^{-1/2} n^{-1} Q_L$, and right plot shows $\rho_n^{-1/2} n^{-1} Q_S$. Dashed vertical line shows bias in simulation. Solid vertical line shows population bias. Solid curve shows population density fit.

discrepancy continues to decrease (not shown), as anticipated by theory. The Louvain clustering method performs moderately well already when the network size is 300, somewhat overestimating the number of clusters, with ARI values less than 0.8 and on average near 0.5. As the network size increases, the clustering and estimated number of clusters approach the ground truth.

4.0.2 Example 2: graphs with $K = 2$, $d = 2$, balanced, disassortative

Consider the dense two-block SBM setting with

$$\mathbf{B} = \begin{bmatrix} 0.30 & 0.75 \\ 0.75 & 0.40 \end{bmatrix}, \quad \boldsymbol{\pi} = \begin{bmatrix} 1/2 \\ 1/2 \end{bmatrix}, \quad n \in \{400, 800, 1000, 4000\}. \quad (14)$$

Graphs generated from this model exhibit so-called disassortative structure, meaning that nodes in different blocks are more likely to be connected than nodes within the same block. For each choice of network size n , simulations are conducted over 1000 independent replications. For $n = 400$, the theoretical values of the parameters are already well estimated by the simulated data per Fig. 3. The Louvain algorithm shows poor performance in detecting clusters which is anticipated and due

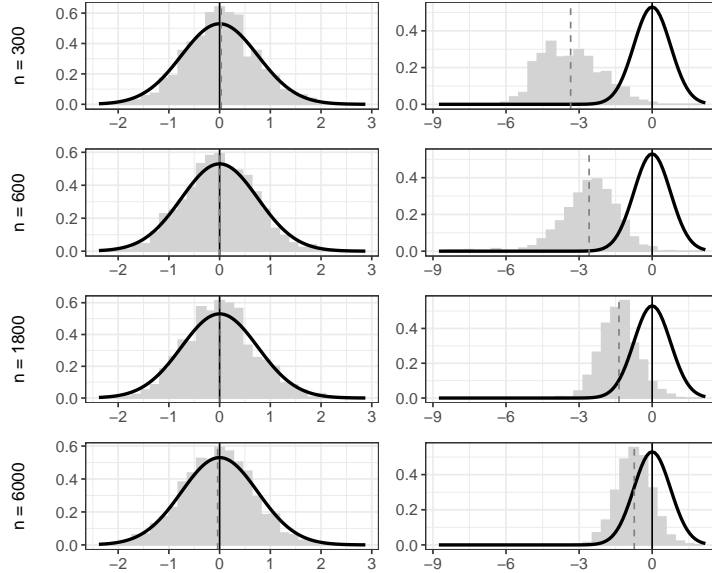


Figure 2: Sparse networks in Section 4.0.1 for $n \in \{300, 600, 1800, 6000\}$ nodes. Left panel shows $\rho_n^{-1/2} n^{-1} Q_L$, and right panel shows $\rho_n^{-1/2} n^{-1} Q_S$. Dashed vertical line shows bias in simulation. Solid vertical line shows population bias. Solid curve shows population density fit.

to the disassortative network connectivity structure. Specifically, the number of detected clusters ranges from five to eleven, with near-zero ARI values.

4.0.3 Example 3: graphs with $K = 2$, $d = 1$, unbalanced, core-periphery

Consider the two-block SBM where \mathbf{B} is rank one of the form $\begin{bmatrix} p \\ q \end{bmatrix} \times \begin{bmatrix} p & q \end{bmatrix}$. Specifically,

$$p = 3/4, q = 1/4, \quad \mathbf{B} = \begin{bmatrix} 0.5625 & 0.1875 \\ 0.1875 & 0.0625 \end{bmatrix}, \quad \boldsymbol{\pi} = \begin{bmatrix} 1/4 \\ 3/4 \end{bmatrix}, \quad n \in \{200, 400, 800, 1000\}, \quad (15)$$

and set $\rho_n = n^{-1/4}$. In this example, \mathbf{B} exhibits core-periphery structure. Fig. 4 shows that even in this sparse setup with relatively small network sizes the simulation performance supports the asymptotic theory. Here simulations are presented for 1000 independent trials, as above. Due to the underlying core-periphery network structure, the Louvain algorithm fails to detect the clusters and always vastly over-estimates the true number of clusters.

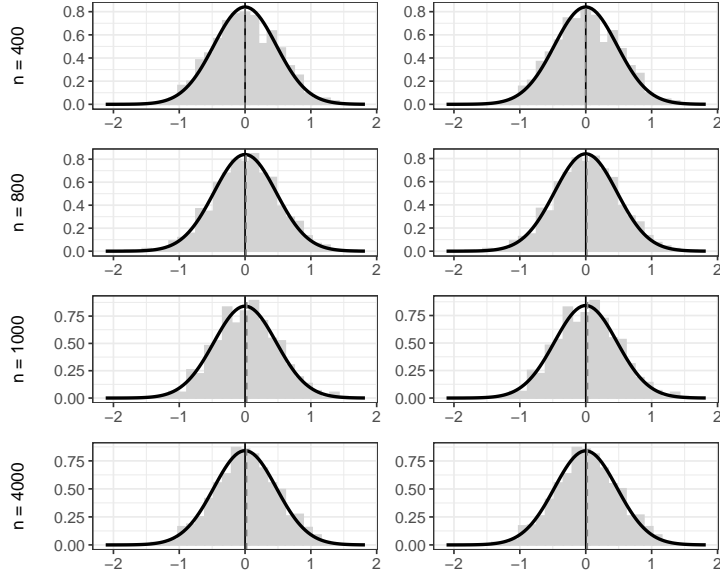


Figure 3: Dense networks in Section 4.0.2 with $n \in \{400, 800, 1000, 4000\}$ nodes. Left panel shows $\rho_n^{-1/2} n^{-1} Q_L$, and right panel shows $\rho_n^{-1/2} n^{-1} Q_S$. Dashed vertical line shows bias in simulation. Solid vertical line shows population bias. Solid curve shows population density fit.

4.0.4 Contour plots and parameter space

This section briefly illustrates how the asymptotic bias and variance of modularity values change as a function of different SBM parameter choices. Two different examples of two-block SBMs are presented, both with $\rho_n \equiv 1$.

In the first example, Fig. 5, \mathbf{B} is of the form $\begin{bmatrix} p \\ q \end{bmatrix} \times \begin{bmatrix} p & q \end{bmatrix}$. Setting $\boldsymbol{\pi} = [1/4, 3/4]^\top$, we plot the asymptotic bias, $\tilde{\boldsymbol{\pi}}^\top \text{vech}(\boldsymbol{\Theta})$, and the asymptotic variances from Theorems 3.1 to 3.3 as functions of (p, q) . In contrast, when setting $\boldsymbol{\pi} = [1/2, 1/2]^\top$, the block-specific biases cancel out to yield an overall bias of zero. This happens because the bias corresponding to the first block, with p^2 , is the negative of that for the second block, with q^2 . This property is exhibited along with the variances in Fig. 6 where we choose $\boldsymbol{\pi} = [0.5001, 0.4999]^\top$. For Q_L , the variance is maximal when both p and q are near 0.75 as exhibited in Fig. 5. For moderately large values of q , the variance may still be large even if p is small which is due to our choice of $\boldsymbol{\pi}$. In contrast, for Q_S , the variance is larger if q is near 0.65 with smaller values of p . The variance corresponding to Q_R increases as p increases when q is near 0.3. As such, loosely speaking, it negotiates the difference between the variances of Q_L and Q_S . Similar observations follow from Fig. 6. Importantly, the balanced block structure in

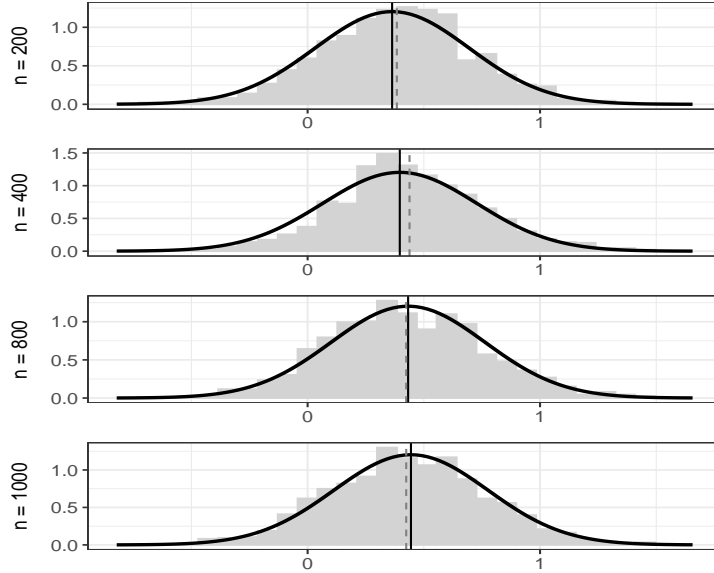


Figure 4: Sparse networks and residual-based modularity in Section 4.0.3. Dashed vertical line shows bias in simulation. Solid vertical line shows population bias. Solid curve shows population density fit.

this scenario induces symmetry in the plots for variances of Q_L , Q_S , and Q_R .

In the second example, Fig. 7, **B** is of the form $\begin{bmatrix} p \\ p^2 \end{bmatrix} \times [p \ p^2]$ and $\boldsymbol{\pi} = [\pi_1, 1 - \pi_1]^\top$. In the same manner we study the asymptotic bias and variances as functions of (p, π_1) . The bias lies approximately in the range from -0.554 to 0.026 , with most values being larger than 0.05 . Irrespective of p , the bias is zero when $\pi_1 = 1/2$ which can be analytically verified in broader generality. We further see that for both Q_L and Q_S , variance is large when p is large and π_1 is close to either zero or one. Their contours exhibit overall similar landscapes. The variance profile of Q_R behaves noticeably differently, exhibiting a single mode near $p = 0.8$, $\pi_1 = 0.4$.

5 Real data analysis

This section applies all three modularity variants to the study of network neuroscience. Each dataset under investigation consists of collections of human brain networks on the same analysis-specific node set but with different edge connectivity properties.

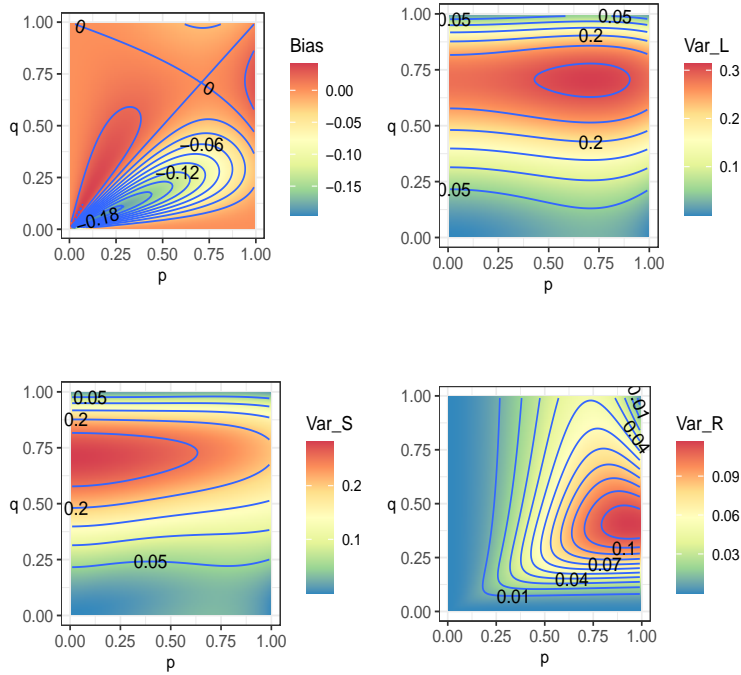


Figure 5: Asymptotic bias and variance plotted as functions of (p, q) where $\mathbf{B} = \begin{bmatrix} p^2 & pq \\ pq & q^2 \end{bmatrix}$ and $\boldsymbol{\pi} = [1/4, 3/4]^\top$.

5.1 Data preliminaries

Modularity is commonly used to explain community structure manifest in anatomical and functional brain connectivity. For example, it has been employed to compare healthy subjects to patients diagnosed with schizophrenia or Alzheimer’s disease (van den Heuvel and Fornito, 2014, Contreras et al., 2019, Zhang et al., 2021). Modularity quantifies the strength of discernible community structure, while the network property known as small-worldness is defined by high local clustering and short global links; thus, a decrease in modularity might also indicate a disruption of small-worldness. Esfahlani et al. (2021) discusses various types of possible null models for different definitions of brain networks and consequent adjustments to the modularity function. Alexander-Bloch et al. (2010) reports reductions in local connectivity and small-worldness in childhood-onset schizophrenia patients. These findings conform with the findings in Bullmore and Sporns (2009) that, compared to healthy individuals, small-world properties seem to degrade in individuals with schizophrenia. Sporns and Betzel (2016) reviews numerous findings on brain networks where func-

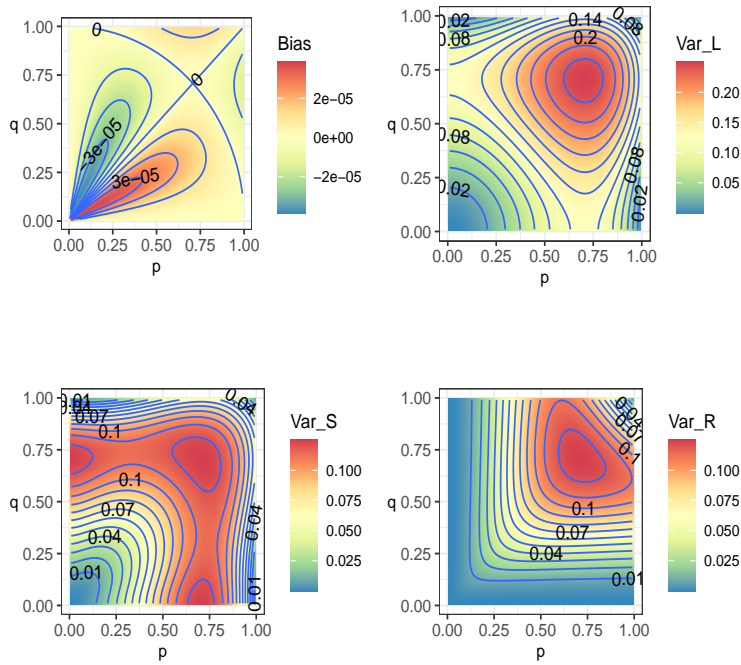


Figure 6: Asymptotic bias and variance plotted as functions of (p, q) where $\mathbf{B} = \begin{bmatrix} p^2 & pq \\ pq & q^2 \end{bmatrix}$ and $\boldsymbol{\pi} = [0.5001, 0.4999]^\top$.

tional correlation networks are treated in different ways and modularity optimization is applied for community detection.

In the study of brain networks, nodes are commonly referred to as regions of interest (ROIs). Aside from the specification of biologically or structurally determined parcellations of brain networks, community structure among ROIs is typically unknown *a priori* and must therefore be inferred. Further, networks derived from brain imaging data typically contain edges with weights and signs (i.e., non-binary, positive or negative). A common technique used to remove seemingly ‘noisy’ or ‘false positive’ edges is to threshold and binarize networks. Among existing approaches, [Bordier et al. \(2017\)](#) considers a percolation-based approach for determining threshold selection. Another technique for obtaining binary graphs is the k -nearest neighbor construction computed on the basis of node feature distances ([von Luxburg, 2007](#)). We, too, must perform binarization in this section as a data preprocessing step.

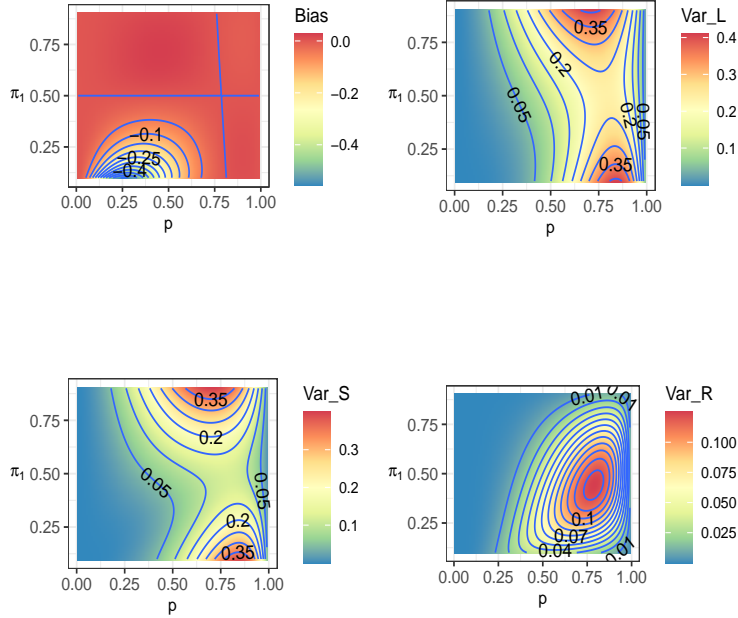


Figure 7: Asymptotic bias and variance plotted as functions of (p, π_1) where $\mathbf{B} = \begin{bmatrix} p^2 & p^3 \\ p^3 & p^4 \end{bmatrix}$ and $\boldsymbol{\pi} = [\pi_1, 1 - \pi_1]^\top$.

5.1.1 COBRE data

We consider the COBRE dataset of brain networks described in Aine et al. (2017) which is freely available in the public database http://fcon_1000.projects.nitrc.org/indi/retro/cobre.html. It consists of networks with 263 regions of interest (ROIs) formed from functional magnetic resonance imaging (fMRI) of brains from (i) 70 healthy control subjects (HC) and (ii) 54 patients with either schizophrenia or schizoaffective disorder (SZ). We make use of the parcellation given by Power et al. (2011) which divides the ROIs into 14 functional brain systems. Specifically, we consider the pre-processed data used in Reli3n et al. (2019) available at <https://github.com/jesusdaniel/graphclass>. By construction, the data are represented by correlation matrices which, after removing the main diagonal, can be viewed as adjacency matrices of loop-free edge-weighted graphs. We entrywise binarize the absolute correlations at the threshold value 0.3, a compromise between removing potentially noisily-observed edges while still preserving the connectivity of all networks in the sample. In particular, this choice derives from the observation that 0.31 and 0.34 are the largest threshold

values preserving connectivity among all healthy controls and patients, respectively. Further, the threshold choice 0.3 corresponds to per-subject absolute correlation percentile values between 75% and 86%.

To establish a baseline, we begin with a more traditional approach to modularity-based analysis using the Newman–Girvan specification, Q_{NG} . For each subject, we run the `leiden()` modularity maximization routine in R for one hundred different seed-based initializations (replicates). As with the Louvain algorithm, the Leiden algorithm is but one of many popular approaches for modularity-based analysis. Doing so yields one hundred partitions of the node set (ROIs) for each subject. The replicate-replicate pairwise ARI values vary between 0.3 and 0.9, indicating sensitivity to initialization and imperfect agreement across replicates, yet they often exceed 0.5 and thus are often not too dissimilar from one another. The corresponding modularity values themselves exhibit heterogeneity per subject, yet almost all subject-specific distributions of modularity values exhibit large negative skew which is consistent with the aim of the underlying algorithm to maximize modularity. Finally, for each subject, we retain their largest Newman–Girvan modularity value and the corresponding partition yielding a node clustering membership vector.

We find that although the mean, median, and standard deviation of the HC modularity values nominally exceed those of the SZ modularity values, their distributions are not significantly different based on a two-sided two-sample Kolmogorov–Smirnov test (p -value > 0.5). Marginally, for both HC and SZ, the distribution of modularity values fails to reject the null hypothesis of normality based on the Shapiro–Wilk test (p -value > 0.25). Further, two-sided t -tests under either the equal or unequal variance specification provide weak evidence that the true difference in means equals zero (p -value > 0.6). These findings are not entirely surprising, given the amount of preprocessing needed for this analysis and the relatively small sample sizes for both controls and patients. Further, the present design and testing setup may also be underpowered.

Next, we examine how the above analysis is impacted by modifying the choice of null network. Our first observation is that Q_{NG} , wherein $P_{ij} = k_i k_j / (2m)$, gives a rank-one choice of null network based on the graph degree profile. On the other hand, the rank-one approximation $\hat{\mathbf{A}} = \hat{\lambda}_1 \hat{\mathbf{u}}_1 \hat{\mathbf{u}}_1^\top$ similarly reflects the degree profile or row sums of \mathbf{A} . Consequently, up to suitable scaling, for this choice of $\hat{\mathbf{A}}$ it is anticipated that $Q_{\text{NG}} \approx Q_{\text{R}}$. Indeed, we observe this behavior for both controls and patients, namely that the rank-one residual-based modularity values do not systematically

differ from Q_{NG} . Further, each marginal distribution of modularity values is not significantly non-Gaussian; this is anticipated on the basis of our theory provided the underlying adjacency matrices are at least approximately block-structured. By choosing to increase the low-rank approximation of \mathbf{A} to dimension two and three, namely by considering Q_{R} with null networks $\sum_{i=1}^2 \widehat{\lambda}_i \widehat{\mathbf{u}}_i \widehat{\mathbf{u}}_i^\top$ and $\sum_{i=1}^3 \widehat{\lambda}_i \widehat{\mathbf{u}}_i \widehat{\mathbf{u}}_i^\top$, respectively, the modularity distributions now appreciably differ from Q_{NG} yet remain approximately Gaussian.

A general challenge facing the use of spectral methods is that between-subject heterogeneity can lead to different estimates for dimensionality, the number of blocks, and block sizes, yielding downstream incompatibilities and complicating comparisons. Indeed, our initial attempts at dimension selection via eigenvalue ratio tests or the method of profile likelihood (Zhu and Ghodsi, 2006) yielded substantial subject-subject differences among controls and patients. Instead, for each network adjacency matrix, we apply the recent method for estimating graph dimension based on cross-validated eigenvalues in Chen et al. (2021) as implemented in the R library `gdim` and function `eigcv()`. This flexible spectral method is designed for approximately low rank and block-structured data yet is not restricted to stochastic blockmodels or even parametric models; it does not cluster the nodes (ROIs) but instead returns the number of informative dimensions (eigenvectors) for input (adjacency) matrices. For both controls and patients, the subject-specific estimated dimension values range from seven to sixteen and concentrate around the values eleven and twelve. This finding is striking and encouraging based on the fact that the underlying Power parcellation (atlas-based partition) divides the ROIs into thirteen known systems and one ‘*Uncertain*’ system but where several systems such as *Cerebellar* and *Memory retrieval* have far fewer nodes than others such as the *Default mode* or *Visual* systems (see the supplement). In the present setting, the *a posteriori* mean, median, and mode estimated dimensionality values for both HC and SZ are closely supported by the *a priori* known Power parcellation partitioning of the 263 brain regions.

On the basis of both the atlas-based parcellation and spectral-based estimated dimensionality of the networks, we next investigate properties of Q_{L} , Q_{S} , and Q_{R} for the COBRE data, reported in Table 2. We begin by computing the per-population average adjacency matrices $\overline{\mathbf{A}}_{\text{HC}}$ and $\overline{\mathbf{A}}_{\text{SZ}}$ along with the corresponding estimated connectivity matrices $\widehat{\mathbf{B}}_{\text{HC}}^{14 \times 14}$ and $\widehat{\mathbf{B}}_{\text{SZ}}^{14 \times 14}$ using τ_{POWER} and supposing that $\rho_n \equiv 1$ (reported behavior is similar for smaller values of ρ_n). We treat these averages as proxies for the corresponding population level quantities $\mathbf{P}_{\text{CLASS}}$ and $\mathbf{B}_{\text{CLASS}}$

Type	\widehat{K}	\widehat{d}	$\widehat{\text{Bias}}$	$\widehat{\sigma}_L^2$	$\widehat{\sigma}_S^2$	$\widehat{\sigma}_R^2$
HC	14	14	0	0.049	0.049	NA
SZ	14	14	0	0.049	0.049	NA
HC	5	5	0	0.105	0.105	NA
SZ	5	5	0	0.107	0.107	NA
HC	5	4	0.025	0.100	0.092	0.005
SZ	5	4	0.041	0.101	0.092	0.006
HC	5	3	0.019	0.097	0.084	0.011
SZ	5	3	0.018	0.098	0.084	0.012

Table 2: Modularity parameter estimates for COBRE data using the Power parcellation. Reported values are rounded.

for $\text{CLASS} \in \{\text{HC}, \text{SZ}\}$. Similarly, τ_{POWER} together with n leads us to write $\pi_{\text{HC}} = \pi_{\text{SZ}}$. On the basis of this block-wise projection with $\widehat{K} = \widehat{d} = 14$, we plug in the estimated connectivity values into our asymptotic formulas to get estimated bias and variance values. Since several of the fourteen communities (systems) have only a few nodes, we further consider a coarser partition of the ROIs by grouping together brain systems (full details provided in the supplement). Doing so yields $\widehat{K} = 5$ blocks, each with more nodes hence larger effective sample sizes. The matrices $\widehat{\mathbf{B}}_{\text{HC}}^{5 \times 5}$ and $\widehat{\mathbf{B}}_{\text{SZ}}^{5 \times 5}$ each have two eigenvalues that are at least one order of magnitude smaller than the largest three eigenvalues, thereby motivating the investigation of rank $\widehat{d} \in \{3, 4, 5\}$ truncations of each connectivity matrix. Overall, Table 2 shows similarities for both populations across different settings, with minor reductions in estimated variability among healthy controls compared to patients.

5.1.2 UK Biobank data

The UK Biobank is “a large-scale biomedical database and research resource containing genetic, lifestyle and health information from half a million UK [United Kingdom] participants” with additional information available at <http://ukbiobank.ac.uk>. We consider resting state fMRI scans for 450 healthy controls (HC) and 469 patients (PT) affected with psychosis, including but not limited to being diagnosed with schizophrenia. We investigate subject-specific networks consisting of 377 ROIs classified into 23 biologically-justified modules (Glasser et al., 2016). The second author’s lab group suggests treating these modules as ‘experimental truths’ or ‘literature truths’, rather than

as ‘ground truths,’ which motivates the analysis herein to avoid directly comparing data-derived partitions to these modules. In the interest of parsimony, we treat 23 as a contextually-informed upper bound on the number of clusters for all networks.

Motivated by [Lei et al. \(2022\)](#), we first Fisher-transform the entries of the functional correlation networks and subsequently obtain binary 50-nearest neighbor networks. This approach produces directed graphs which are subsequently symmetrized such that two nodes are connected when at least one of them is a nearest neighbor of the other. Across all healthy controls, node degrees take values in the interval [86, 161], whereas the corresponding interval for patients is [90, 155].

For the sake of benchmarking, we first examine the properties of Q_{NG} using the `leiden()` modularity maximization routine across twenty different initializations per subject, keeping the largest modularity value and corresponding partition (node clustering) for each. We find that the mean and median modularity values are nominally larger for the healthy control group than for the patient group; further, the standard deviation of modularity is nominally smaller for the healthy control group. However, the modularity distributions are not significantly different based on a two-sided two-sample Kolmogorov–Smirnov test (p -value > 0.7); neither distribution fails to reject normality based on the Shapiro–Wilk test (p -values > 0.05), and the distributions display an insignificant difference in means based on a two-sample t -test (p -value > 0.8). These preliminary investigations provide weak evidence of differences in modularity values between groups.

Here, the `leiden()` clustering algorithm returns $\hat{K} \in \{5, 6\}$ across both healthy controls and patients, each with mode equal to 5. Using the R library `gdim` and function `eigcv()` yields estimated graph dimension values $\{11, \dots, 15\}$ for controls and $\{11, \dots, 16\}$ for patients, each with mode equal to 13 and second-most-frequent value equal to 14. Interestingly, here $\hat{K} < \hat{d}$ which lies outside the set of possibilities for stochastic blockmodel graphs. Nevertheless, we can still ask about the behavior of Q_{R} for $\hat{d} = 5$. In particular, we consider two choices for $\hat{\tau}$, the first based on clustering with `leiden()`, and the second based on Gaussian mixture model clustering with five components applied to the leading \hat{K} eigenvectors of each adjacency matrix, using the R functionality `Mclust()`. [Fig. 8](#) displays the results, showing that unlike above, here the distributions of modularity values significantly deviate from normality, yet the distributional differences between groups are not appreciably different for either clustering method.

Our analysis suggests that the control sample is not significantly different from the patient sam-

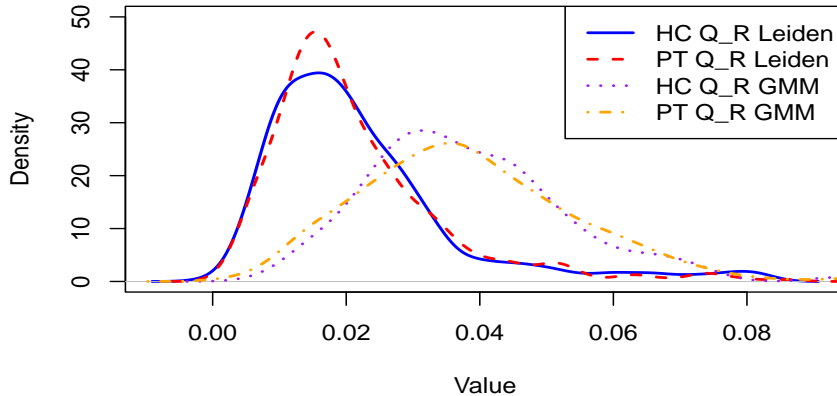


Figure 8: Estimated residual-based modularity densities for the UK Biobank for different choices of node clustering.

ple in terms of several modularity-based characteristics. This conclusion is somewhat expected and agrees with precedent, given that (i) the data are from resting state fMRI rather than task-based fMRI and that (ii) the patient population is aggregated across different, varied psychosis diagnoses, which include the following classifications: schizophrenia, schizoaffective disorder, recurrent depression, manic episodes, bipolar disorder, and unusual psychotic experience. Our findings are in terms of multiple approaches to modularity-based analysis, rather than just a single modularity criterion, enabling nuance and inquiry from different points of view.

6 Discussion

The findings in this paper can be readily applied together with existing results for stochastic blockmodel graphs and their known statistical properties. For example, [Lei \(2016\)](#) establishes a goodness of fit criterion for determining the number of communities in SBM graphs. [Tang et al. \(2022\)](#) provides a comparison of likelihood and spectral approaches for SBM parameter estimation. [Zhang et al. \(2022\)](#) provides guarantees for large-scale, randomized SBM analysis. Further, SBM model selection can in principle be carried out on observed data via the network cross-validation approach in [Chen and Lei \(2018\)](#) or the edge cross-validation approach in [Li et al. \(2020\)](#), though these methods do not reach a consensus when applied to our data. Of note, recent years have

witnessed significant advances regarding the problem of estimating the number of communities K in network models (Jin et al., 2023, Han et al., 2023, Chen et al., 2021, Hwang et al., 2023). Moving forward, these developments can conceivably be incorporated in the ongoing study of modularity and its variants, thereby avoiding the problematic yet still oft-posed assumption that K is known.

In practice, the choice of modularity variant *may* or arguably necessarily *should* be application-dependent, a sentiment shared in Bazzi et al. (2016). Here we strive for illustrations, rather than definitive analysis of any one particular dataset, hence we consider multiple modularity variants in tandem. Even when faced with relatively small networks, asymptotics may still be useful as we have attempted to demonstrate.

Of course, blockmodels are not themselves the end goal when investigating complex networks. Nevertheless, they offer a tractable starting point for investigating and developing statistical foundations. Encouragingly, (at least) approximate block structure is often observed empirically or biologically plausible and can be productively leveraged to unify theory, methods, and practice (Priebe et al., 2019).

Supplementary materials

Appendix: Document containing proofs of results in the article, additional simulation examples, and further discussion of the data analysis.

R code and data: Code to reproduce the simulations and real data analysis in the article, subject to data sharing permission.

References

- Emmanuel Abbe. Community detection and stochastic block models: recent developments. *Journal of Machine Learning Research*, 18(177):1–86, 2018. URL <http://jmlr.org/papers/v18/16-480.html>.
- Christopher Aicher, Abigail Z. Jacobs, and Aaron Clauset. Learning latent block structure in weighted networks. *Journal of Complex Networks*, 3(2):221–248, Jun 2014. doi: 10.1093/comnet/cnu026. URL <https://doi.org/10.1093%2Fcomnet%2Fcnu026>.
- Christopher Aicher, Abigail Z. Jacobs, and Aaron Clauset. Adapting the stochastic block model to edge-weighted networks. *ArXiv*, abs/1305.5782, 2013.
- CJ Aine, Henry Jeremy Bockholt, Juan R Bustillo, José M Cañive, Arvind Caprihan, Charles Gasparovic, Faith M. Hanlon, Jon M. Houck, Rex E. Jung, and John Lauriello. Multimodal neuroimaging in schizophrenia: description and dissemination. *Neuroinformatics*, 15(4):343–364, 2017. doi: 10.1007/s12021-017-9338-9. URL <https://www.ncbi.nlm.nih.gov/pmc/articles/PMC5671541/>.
- Edoardo M. Airoldi, David M. Blei, Stephen E. Fienberg, and Eric P. Xing. Mixed membership stochastic blockmodels. *Journal of Machine Learning Research*, 9(65):1981–2014, 2008. URL <http://jmlr.org/papers/v9/airoldi08a.html>.
- Aaron F. Alexander-Bloch, Nitin Gogtay, David Meunier, Rasmus Birn, Liv Clasen, Francois Lalonde, Rhoshel Lenroot, Jay Giedd, and Edward T. Bullmore. Disrupted modularity and local connectivity of brain functional networks in childhood-onset schizophrenia. *Frontiers in Systems Neuroscience*, 4(147):1–16, 2010. ISSN 1662-5137. doi: 10.3389/fnsys.2010.00147. URL <https://www.ncbi.nlm.nih.gov/pubmed/21031030>.
- Avanti Athreya, Minh Tang, Youngser Park, and Carey E. Priebe. On estimation and inference in latent structure random graphs. *Statistical Science*, 36(1):68–88, 2021. doi: 10.1214/20-STS787. URL <https://doi.org/10.1214/20-STS787>.
- Marya Bazzi, Mason A. Porter, Stacy Williams, Mark McDonald, Daniel J. Fenn, and Sam D. Howison. Community detection in temporal multilayer networks, with an application to correla-

tion networks. *Multiscale Modeling & Simulation*, 14(1):1–41, 2016. doi: 10.1137/15M1009615. URL <https://epubs.siam.org/doi/10.1137/15M1009615>.

Sharmodeep Bhattacharyya and Shirshendu Chatterjee. General community detection with optimal recovery conditions for multi-relational sparse networks with dependent layers. *ArXiv*, abs/2004.03480, 2020.

Peter J. Bickel and Aiyou Chen. A nonparametric view of network models and Newman–Girvan and other modularities. *Proceedings of the National Academy of Sciences*, 106(50):21068–21073, 2009.

Peter J. Bickel, David Choi, Xiangyu Chang, and Hai Zhang. Asymptotic normality of maximum likelihood and its variational approximation for stochastic blockmodels. *The Annals of Statistics*, 41(4):1922–1943, 2013. doi: 10.1214/13-AOS1124. URL <https://doi.org/10.1214/13-AOS1124>.

Vincent Blondel, Gautier Krings, and Isabelle Thomas. Regions and borders of mobile telephony in Belgium and in the Brussels metropolitan zone. *Brussels Studies*, 42:1–12, 10 2010. doi: 10.4000/brussels.806. URL <https://journals.openedition.org/brussels/806>.

Vincent D. Blondel, Jean-Loup Guillaume, Renaud Lambiotte, and Etienne Lefebvre. Fast unfolding of communities in large networks. *Journal of Statistical Mechanics: Theory and Experiment*, 2008(10):10008, Oct 2008. doi: 10.1088/1742-5468/2008/10/p10008. URL <https://doi.org/10.1088/1742-5468/2008/10/p10008>.

Béla Bollobás, Svante Janson, and Oliver Riordan. The phase transition in inhomogeneous random graphs. *Random Structures and Algorithms*, 31(1):3–122, 2007. doi: 10.1002/rsa.20168. URL <https://doi.org/10.1002/rsa.20168>.

Cecile Bordier, Carlo Nicolini, and Angelo Bifone. Graph analysis and modularity of brain functional connectivity networks: Searching for the optimal threshold. *Frontiers in Neuroscience*, 11(441):1–9, 2017. ISSN 1662-4548. doi: doi.org/10.3389/fnins.2017.00441. URL <https://www.ncbi.nlm.nih.gov/pubmed/28824364>.

- Ulrik Brandes, Daniel Delling, Marco Gaertler, Robert Gorke, Martin Hoefer, Zoran Nikoloski, and Dorothea Wagner. On modularity clustering. *IEEE Transactions on Knowledge and Data Engineering*, 20(2):172–188, 2008. doi: 10.1109/TKDE.2007.190689. URL <https://ieeexplore.ieee.org/document/4358966>.
- Ed Bullmore and Olaf Sporns. Complex brain networks: graph theoretical analysis of structural and functional systems. *Nature Reviews Neuroscience*, 10(3):186–98, 2009. doi: 10.1038/nrn2575. URL <https://www.ncbi.nlm.nih.gov/pubmed/19190637>.
- Emidio Capriotti, Kivilcim Ozturk, and Hannah Carter. Integrating molecular networks with genetic variant interpretation for precision medicine. *Wiley Interdisciplinary Reviews: Systems Biology and Medicine*, 11(3):e1443, 2019. doi: 10.1002/wsbm.1443. URL <https://www.ncbi.nlm.nih.gov/pmc/articles/PMC6450710/>.
- Fan Chen, Sebastien Roch, Karl Rohe, and Shuqi Yu. Estimating graph dimension with cross-validated eigenvalues. *arXiv preprint arXiv:2108.03336*, 2021.
- Kehui Chen and Jing Lei. Network cross-validation for determining the number of communities in network data. *Journal of the American Statistical Association*, 113(521):241–251, 2018. doi: 10.1080/01621459.2016.1246365. URL <https://www.tandfonline.com/doi/full/10.1080/01621459.2016.1246365>.
- Aaron Clauset, Mark E. J. Newman, and Cristopher Moore. Finding community structure in very large networks. *Physical Review E*, 70(6):066111, Dec 2004. doi: 10.1103/PhysRevE.70.066111. URL <https://link.aps.org/doi/10.1103/PhysRevE.70.066111>.
- Joey A. Contreras, Andrea Avena-Koenigsberger, Shannon L. Risacher, John D. West, Eileen Tallman, Brenna C. McDonald, Martin R. Farlow, Liana G. Apostolova, Joaquín Goñi, Mario Dziedzic, Yu-Chien Wu, Daniel Kessler, Lucas Jeub, Santo Fortunato, Andrew J. Saykin, and Olaf Sporns. Resting state network modularity along the prodromal late onset alzheimer’s disease continuum. *NeuroImage: Clinical*, 22:101687, 2019.
- Manlio De Domenico. Multilayer modeling and analysis of human brain networks. *Gigascience*,

6:1–8, 2017. doi: doi:10.1093/gigascience/gix004. URL <https://www.ncbi.nlm.nih.gov/pmc/articles/PMC5437946/>.

Manlio De Domenico, Andrea Lancichinetti, Alex Arenas, and Martin Rosvall. Identifying modular flows on multilayer networks reveals highly overlapping organization in interconnected systems. *Physical Review X*, 5(1):011027, Mar 2015a. doi: 10.1103/PhysRevX.5.011027. URL <https://link.aps.org/doi/10.1103/PhysRevX.5.011027>.

Manlio De Domenico, Vincenzo Nicosia, Alexandre Arenas, and Vito Latora. Structural reducibility of multilayer networks. *Nature Communications*, 6(1):6864, Apr 2015b. ISSN 2041-1723. doi: 10.1038/ncomms7864. URL <https://doi.org/10.1038/ncomms7864>.

Xiaowen Dong, Pascal Frossard, P. Vandergheynst, and N. Nefedov. Clustering with multi-layer graphs: a spectral perspective. *IEEE Transactions on Signal Processing*, 60(11):5820–5831, Nov 2012. doi: 10.1109/tsp.2012.2212886. URL <http://dx.doi.org/10.1109/TSP.2012.2212886>.

Jordi Duch and Alex Arenas. Community detection in complex networks using extremal optimization. *Physical Review E*, 72:027104, Aug 2005. doi: 10.1103/PhysRevE.72.027104. URL <https://link.aps.org/doi/10.1103/PhysRevE.72.027104>.

Paul Erdős and Alfred Rényi. On random graphs i. *Publicationes Mathematicae Debrecen*, 6: 290–297, 1959.

Farnaz Z. Esfahlani, Youngheun Jo, Maria G. Puxeddu, Haily Merritt, Jacob C. Tanner, Sarah Greenwell, Riya Patel, Joshua Faskowitz, and Richard F. Betzel. Modularity maximization as a flexible and generic framework for brain network exploratory analysis. *Neuroimage*, 244:118607, 2021. ISSN 1095-9572. doi: 10.1016/j.neuroimage.2021.118607. URL <https://www.ncbi.nlm.nih.gov/pubmed/34607022>.

Heinz Eulau and Jonathan W. Siegel. Social network analysis and political behavior: A feasibility study. *The Western Political Quarterly*, 34(4):499–509, 1981. doi: 10.2307/447464. URL <http://www.jstor.org/stable/447464>.

Jianqing Fan, Yingying Fan, Xiao Han, and Jinchi Lv. Asymptotic theory of eigenvectors for

- random matrices with diverging spikes. *Journal of the American Statistical Association*, 117 (538):996–1009, 2022.
- Courtney L. Fitzpatrick, Elizabeth A. Hobson, Tamra C. Mendelson, Rafael L. Rodríguez, Rebecca J. Safran, Elizabeth S. C. Scordato, Maria R. Servedio, Caitlin A. Stern, Laurel B. Symes, and Michael Kopp. Theory meets empiry: A citation network analysis. *BioScience*, 68(10): 805–812, 08 2018. ISSN 0006-3568. doi: 10.1093/biosci/biy083. URL <https://doi.org/10.1093/biosci/biy083>.
- Zoltán Füredi and János Komlós. The eigenvalues of random symmetric matrices. *Combinatorica*, 1:233–241, 1981.
- Edgar N. Gilbert. Random Graphs. *The Annals of Mathematical Statistics*, 30(4):1141 – 1144, 1959. doi: 10.1214/aoms/1177706098. URL <https://doi.org/10.1214/aoms/1177706098>.
- Matthew F. Glasser, Timothy S. Coalson, Emma C. Robinson, Carl D. Hacker, John Harwell, Essa Yacoub, Kamil Ugurbil, Jesper Andersson, Christian F Beckmann, and Mark Jenkinson. A multi-modal parcellation of human cerebral cortex. *Nature*, 536(7615):171–178, 2016. URL <https://www.nature.com/articles/nature18933>.
- David S. Grayson and Damien A. Fair. Development of large-scale functional networks from birth to adulthood: a guide to the neuroimaging literature. *Neuroimage*, 160:15–31, 2017. doi: 10.1016/j.neuroimage.2017.01.079. URL <https://www.ncbi.nlm.nih.gov/pmc/articles/PMC5538933/>.
- R. Guimerà, S. Mossa, A. Turtschi, and L. A. N. Amaral. The worldwide air transportation network: anomalous centrality, community structure, and cities’ global roles. *Proceedings of the National Academy of Sciences*, 102(22):7794–7799, 2005. doi: 10.1073/pnas.0407994102. URL <https://www.pnas.org/doi/abs/10.1073/pnas.0407994102>.
- Xiao Han, Qing Yang, and Yingying Fan. Universal rank inference via residual subsampling with application to large networks. *The Annals of Statistics*, 51(3):1109–1133, 2023. doi: 10.1214/23-AOS2282. URL <https://doi.org/10.1214/23-AOS2282>.
- Paul W. Holland, Kathryn Blackmond Laskey, and Samuel Leinhardt. Stochastic blockmodels: first steps. *Social Networks*, 5(2):109–137, 1983. ISSN 0378-8733. doi: [https://doi.org/10.1016/0378-8733\(83\)90057-9](https://doi.org/10.1016/0378-8733(83)90057-9).

org/10.1016/0378-8733(83)90021-7. URL <https://www.Elsevier.com/science/article/pii/0378873383900217>.

Lawrence Hubert and Phipps Arabie. Comparing partitions. *Journal of Classification*, 2(1):193–218, 12 1985. doi: 10.1007/BF01908075. URL <https://doi.org/10.1007/BF01908075>.

Neil Hwang, Jiarui Xu, Shirshendu Chatterjee, and Sharmodeep Bhattacharyya. On the estimation of the number of communities for sparse networks. *Journal of the American Statistical Association*, pages 1–16, 2023. doi: 10.1080/01621459.2023.2223793. URL <https://doi.org/10.1080/01621459.2023.2223793>.

Jiashun Jin, Zheng Tracy Ke, Shengming Luo, and Minzhe Wang. Optimal estimation of the number of network communities. *Journal of the American Statistical Association*, 118(543):2101–2116, 2023. doi: 10.1080/01621459.2022.2035736. URL <https://doi.org/10.1080/01621459.2022.2035736>.

Brian Karrer and Mark E. J. Newman. Stochastic blockmodels and community structure in networks. *Physical Review E*, 83(1):016107, Jan 2011. doi: 10.1103/PhysRevE.83.016107. URL <https://link.aps.org/doi/10.1103/PhysRevE.83.016107>.

Florian Klimm, Nick S. Jones, and Michael T. Schaub. Modularity maximization for graphons. *SIAM Journal on Applied Mathematics*, 82(6):1930–1952, 2022. doi: 10.1137/22M1492003. URL <https://doi.org/10.1137/22M1492003>.

John Koo, Minh Tang, and Michael W. Trosset. Popularity adjusted block models are generalized random dot product graphs. *Journal of Computational and Graphical Statistics*, 32(1):131–144, 2023. doi: 10.1080/10618600.2022.2081576. URL <https://doi.org/10.1080/10618600.2022.2081576>.

Clement Lee and Darren J. Wilkinson. A review of stochastic block models and extensions for graph clustering. *Applied Network Science*, 4(1):1–50, Dec 2019. doi: 10.1007/s41109-019-0232-2. URL <https://appliednetsci.springeropen.com/articles/10.1007/s41109-019-0232-2>.

Du Lei, Kun Qin, Walter H. L. Pinaya, Jonathan Young, Therese Van Amelsvoort, Machteld Marcelis, Gary Donohoe, David O. Mothersill, Aiden Corvin, Sandra Vieira, Su Lui, Cristina

- Scarpazza, Celso Arango, Ed Bullmore, Qiyong Gong, Philip McGuire, and Andrea Mechelli. Graph convolutional networks reveal network-level functional dysconnectivity in schizophrenia. *Schizophrenia Bulletin*, 48(4):881–892, 05 2022. doi: 10.1093/schbul/sbac047. URL <https://doi.org/10.1093/schbul/sbac047>.
- Jing Lei. A goodness-of-fit test for stochastic block models. *The Annals of Statistics*, 44(1):401–424, 2016. doi: 10.1214/15-AOS1370. URL <https://doi.org/10.1214/15-AOS1370>.
- Jing Lei, Kehui Chen, and Brian Lynch. Consistent community detection in multi-layer network data. *Biometrika*, 107(1):61–73, 2019. doi: 10.1093/biomet/asz068. URL <https://doi.org/10.1093/biomet/asz068>.
- Carson Kai-Sang Leung, Syed K. Tanbeer, and Juan J. Cameron. Interactive discovery of influential friends from social networks. *Social Network Analysis and Mining*, 4(1):1–13, 02 2014. ISSN 1869-5469. doi: 10.1007/s13278-014-0154-z. URL <https://link.springer.com/article/10.1007/s13278-014-0154-z>.
- Tianxi Li, Elizaveta Levina, and Ji Zhu. Network cross-validation by edge sampling. *Biometrika*, 107(2):257–276, 04 2020. ISSN 0006-3444. doi: 10.1093/biomet/asaa006. URL <https://doi.org/10.1093/biomet/asaa006>.
- Yang Li and Yongcheng Qi. Asymptotic distribution of modularity in networks. *Metrika*, 83(4):467–484, May 2020. ISSN 0026-1335. doi: 10.1007/s00184-019-00740-7. URL <https://link.springer.com/content/pdf/10.1007/s00184-019-00740-7.pdf>.
- Vince Lyzinski, Daniel L. Sussman, Minh Tang, Avanti Athreya, and Carey E. Priebe. Perfect clustering for stochastic blockmodel graphs via adjacency spectral embedding. *Electronic Journal of Statistics*, 8(2):2905–2922, 2014. doi: 10.1214/14-EJS978. URL <https://doi.org/10.1214/14-EJS978>.
- Rong Ma and Ian Barnett. The asymptotic distribution of modularity in weighted signed networks. *Biometrika*, 108(1):1–16, Jul 2020. doi: 10.1093/biomet/asaa059. URL <https://www.ncbi.nlm.nih.gov/pmc/articles/PMC8300091/>.

- Jan R. Magnus and Heinz Neudecker. The elimination matrix: Some lemmas and applications. *SIAM Journal on Algebraic Discrete Methods*, 1(4):422–449, 1980. doi: 10.1137/0601049. URL <https://doi.org/10.1137/0601049>.
- Peter J. Mucha, Thomas Richardson, Kevin Macon, Mason A. Porter, and Jukka-Pekka Onnela. Community structure in time-dependent, multiscale, and multiplex networks. *Science*, 328(5980): 876–878, May 2010. ISSN 1095-9203. doi: 10.1126/science.1184819. URL <http://dx.doi.org/10.1126/science.1184819>.
- Mark E. J. Newman. Fast algorithm for detecting community structure in networks. *Physical Review E*, 69:066133, Jun 2004. doi: 10.1103/PhysRevE.69.066133. URL <https://link.aps.org/doi/10.1103/PhysRevE.69.066133>.
- Mark E. J. Newman. Finding community structure in networks using the eigenvectors of matrices. *Physical Review E*, 74(3):036104, Sep 2006a. doi: 10.1103/PhysRevE.74.036104. URL <https://link.aps.org/doi/10.1103/PhysRevE.74.036104>.
- Mark E. J. Newman. Modularity and community structure in networks. *Proceedings of the National Academy of Sciences*, 103(23):8577–8582, 2006b. doi: 10.1073/pnas.0601602103. URL <https://www.pnas.org/content/103/23/8577.full.pdf>.
- Mark E. J. Newman. *Networks*. Oxford University Press, 2 edition, 2018. doi: 10.1093/oso/9780198805090.001.0001.
- Mark E. J. Newman and Michelle Girvan. Finding and evaluating community structure in networks. *Physical Review E*, 69(2):026113, Feb 2004. doi: 10.1103/PhysRevE.69.026113. URL <https://link.aps.org/doi/10.1103/PhysRevE.69.026113>.
- Mason A. Porter, Peter J. Mucha, Mark E. J. Newman, and Casey M. Warmbrand. A network analysis of committees in the U.S. House of Representatives. *Proceedings of the National Academy of Sciences*, 102(20):7057–7062, 2005. doi: 10.1073/pnas.0500191102. URL <https://www.pnas.org/doi/abs/10.1073/pnas.0500191102>.
- Jonathan D. Power, Alexander L. Cohen, Steven M. Nelson, Gagan S. Wig, Kelly Anne Barnes, Jessica A. Church, Alecia C. Vogel, Timothy O. Laumann, Fran M. Miezin, Bradley L. Schlaggar,

- and Steven E. Petersen. Functional network organization of the human brain. *Neuron*, 72(4): 665–678, 2011. doi: 10.1016/j.neuron.2011.09.006. URL <https://www.ncbi.nlm.nih.gov/pmc/articles/PMC3222858/>.
- Carey E. Priebe, Youngser Park, Joshua T. Vogelstein, John M. Conroy, Vince Lyzinski, Minh Tang, Avanti Athreya, Joshua Cape, and Eric Bridgeford. On a two-truths phenomenon in spectral graph clustering. *Proceedings of the National Academy of Sciences*, 116(13):5995–6000, 2019. ISSN 0027-8424. doi: 10.1073/pnas.1814462116. URL <https://www.pnas.org/content/116/13/5995>.
- Jörg Reichardt and Stefan Bornholdt. Statistical mechanics of community detection. *Physical Review E*, 74:016110, Jul 2006. doi: 10.1103/PhysRevE.74.016110. URL <https://link.aps.org/doi/10.1103/PhysRevE.74.016110>.
- Jesús D. Arroyo Relión, Daniel Kessler, Elizaveta Levina, and Stephan F. Taylor. Network classification with applications to brain connectomics. *The Annals of Applied Statistics*, 13(3):1648–1677, Sep 2019. doi: 10.1214/19-aos1252. URL <https://doi.org/10.1214%2F19-aos1252>.
- Patrick Rubin-Delanchy, Joshua Cape, Minh Tang, and Carey E. Priebe. A statistical interpretation of spectral embedding: the generalised random dot product graph. *Journal of the Royal Statistical Society Series B*, 84(4):1446–1473, September 2022. doi: 10.1111/rssb.12509. URL <https://academic.oup.com/jrssb/article/84/4/1446/7073272>.
- Mikhail Rubinov and Olaf Sporns. Complex network measures of brain connectivity: uses and interpretations. *Neuroimage*, 52(3):1059–1069, 2010. doi: 10.1016/j.neuroimage.2009.10.003. URL <https://www.Elsevier.com/science/article/pii/S105381190901074X?via%3Dihub>.
- Srijan Sengupta and Yuguo Chen. A block model for node popularity in networks with community structure. *Journal of the Royal Statistical Society Series B*, 80(2):365–386, March 2018. doi: 10.1111/rssb.12245. URL <https://ideas.repec.org/a/bla/jorssb/v80y2018i2p365-386.html>.
- Olaf Sporns and Richard F. Betzel. Modular brain networks. *Annual Review of Psychology*, 67:1–30, 2016. ISSN 1545-2085. doi: 10.1146/annurev-psych-122414-033634. URL <https://www.ncbi.nlm.nih.gov/pubmed/26393868>.

- Tracy M. Sweet. Incorporating covariates into stochastic blockmodels. *Journal of Educational and Behavioral Statistics*, 40(6):635–664, 2015. doi: 10.3102/1076998615606110. URL <https://journals.sagepub.com/doi/10.3102/1076998615606110>.
- Aidi Tan, Huiya Huang, Peng Zhang, and Shao Li. Network-based cancer precision medicine: a new emerging paradigm. *Cancer Letters*, 458:39–45, 2019. doi: 10.1016/j.canlet.2019.05.015. URL <https://www.Elsevier.com/science/article/pii/S0304383519303106?via%3Dihub>.
- Minh Tang, Joshua Cape, and Carey E. Priebe. Asymptotically efficient estimators for stochastic blockmodels: the naive MLE, the rank-constrained MLE, and the spectral estimator. *Bernoulli*, 28(2):1049–1073, 2022. doi: 10.3150/21-BEJ1376. URL <https://doi.org/10.3150/21-BEJ1376>.
- Vincent A. Traag, Ludo Waltman, and Nees Jan van Eck. From Louvain to Leiden: guaranteeing well-connected communities. *Scientific Reports*, 9(1):5233, Mar 2019. doi: 10.1038/s41598-019-41695-z. URL <https://www.nature.com/articles/s41598-019-41695-z>.
- Martijn P. van den Heuvel and Alex Fornito. Brain networks in schizophrenia. *Neuropsychology Review*, 24:32–48, 2014.
- Ulrike von Luxburg. A tutorial on spectral clustering. *Statistics and Computing*, 17(4):395–416, Dec 2007. doi: 10.1007/s11222-007-9033-z. URL <https://doi.org/10.1007/s11222-007-9033-z>.
- Fangzheng Xie. Entrywise limit theorems of eigenvectors for signal-plus-noise matrix models with weak signals. *Bernoulli*, 30(1):388–418, 2022. doi: 10.3150/23-BEJ1602. URL <https://doi.org/10.3150/23-BEJ1602>.
- Fangzheng Xie and Yanxun Xu. Efficient estimation for random dot product graphs via a one-step procedure. *Journal of the American Statistical Association*, 118(541):651–664, 2023. doi: 10.1080/01621459.2021.1948419. URL <https://doi.org/10.1080/01621459.2021.1948419>.
- Wayne W. Zachary. An information flow model for conflict and fission in small groups. *Journal of Anthropological Research*, 33(4):452–473, 1977. ISSN 00917710. doi: 10.1086/jar.33.4.3629752. URL <http://www.jstor.org/stable/3629752>.

- Hai Zhang, Xiao Guo, and Xiangyu Chang. Randomized spectral clustering in large-scale stochastic block models. *Journal of Computational and Graphical Statistics*, 31(3):887–906, 2022. doi: 10.1080/10618600.2022.2034636. URL <https://www.tandfonline.com/doi/abs/10.1080/10618600.2022.2034636>.
- Jingfei Zhang and Yuguo Chen. A hypothesis testing framework for modularity based network community detection. *Statistica Sinica*, 27(1):437–456, 2017. ISSN 1545-2085. doi: 10.5705/ss.202015.0040. URL <http://www.jstor.org/stable/44114379>.
- Yangyang Zhang, Xiao Jiang, Lishan Qiao, and Mingxia Liu. Modularity-guided functional brain network analysis for early-stage dementia identification. *Frontiers in Neuroscience*, 15:720909, 2021.
- Yun Zhang, Kehui Chen, Allan Sampson, Kai Hwang, and Beatriz Luna. Node features adjusted stochastic block model. *Journal of Computational and Graphical Statistics*, 28(2):362–373, 2019. doi: 10.1080/10618600.2018.1530117. URL <https://www.tandfonline.com/doi/full/10.1080/10618600.2018.1530117>.
- Mu Zhu and Ali Ghodsi. Automatic dimensionality selection from the scree plot via the use of profile likelihood. *Computational Statistics & Data Analysis*, 51(2):918–930, 2006. ISSN 0167-9473. doi: <https://doi.org/10.1016/j.csda.2005.09.010>. URL <https://www.Elsevier.com/science/article/pii/S0167947305002343>.

A Appendix to “On inference for modularity statistics in structured networks” by Anirban Mitra, Konasale Prasad, and Joshua Cape

This document contains proofs of the stated theorems, additional simulation examples, and further discussion pertaining to the real data analysis.

A.1 Proofs of asymptotic normality

Lemma A.1 (Bickel et al. (2013)). *For $n \geq 1$, suppose $\mathbf{A}^{(n)} \sim \text{SBM}(\mathbf{B}, \boldsymbol{\pi})$ is a sequence of stochastic blockmodel graphs with sparsity factor ρ_n satisfying $n\rho_n = \omega(\log n)$. Let $\mathbf{B}^{(L)} = (B_{kl}^{(L)})$ be as in Definition 3.2. Then, as $n \rightarrow \infty$,*

$$n\rho_n^{1/2} \text{vech}(\widehat{\mathbf{B}}^{(L)} - \mathbf{B}) \xrightarrow{d} \mathcal{N}(\mathbf{0}, \mathbf{D}^{-1}). \quad (16)$$

The diagonal matrix $\mathbf{D} = (\mathbf{D}^{-1})^{-1}$ is defined in Eq. (5) of the main text.

Lemma A.2 (Tang et al. (2022)). *For $n \geq 1$, suppose $\mathbf{A}^{(n)} \sim \text{SBM}(\mathbf{B}, \boldsymbol{\pi})$ is a sequence of stochastic blockmodel graphs with sparsity factor ρ_n satisfying $n\rho_n = \omega(\sqrt{n})$. Let $\widehat{\mathbf{B}}^{(S)} = (\widehat{B}_{kl}^{(S)})$ be as in Definition 3.2. Then, as $n \rightarrow \infty$,*

$$n\rho_n^{1/2} \text{vech}(\widehat{\mathbf{B}}^{(S)} - \mathbf{B}) - \rho_n^{-1/2} \text{vech}(\boldsymbol{\Theta}) \xrightarrow{d} \mathcal{N}(\mathbf{0}, \widetilde{\boldsymbol{\Gamma}}). \quad (17)$$

Here, $\boldsymbol{\Theta}$ per Eq. (7) is the asymptotic bias and $\widetilde{\boldsymbol{\Gamma}}$ per Eq. (8) is the asymptotic covariance matrix.

Importantly, Tang et al. (2022) establishes the decomposition

$$\begin{aligned} & n\rho_n^{1/2} \text{vech} \left(\widehat{\mathbf{B}}^{(S)} - \mathbf{B} - (n\rho_n)^{-1} \boldsymbol{\Theta} \right) \\ &= n\rho_n^{1/2} \mathcal{L}_K (\mathbf{I} - \check{\check{\boldsymbol{\Pi}}}_{\mathbf{V}}^{\perp} \otimes \check{\check{\boldsymbol{\Pi}}}_{\mathbf{V}}^{\perp}) \mathcal{D}_K \text{vech}(\widehat{\mathbf{B}}^{(L)} - \mathbf{B}) + O_{\mathbb{P}} \left(n^{-1/2} \rho_n^{-1} \right). \end{aligned} \quad (18)$$

In Eq. (18), $\check{\check{\boldsymbol{\Pi}}}_{\mathbf{V}}^{\perp} = \mathbf{I} - \mathbf{V}(\mathbf{V}^{\top} \mathbf{Z}^{\top} \mathbf{Z} \mathbf{V})^{-1} \mathbf{V}^{\top} \mathbf{Z}^{\top} \mathbf{Z}$ and therefore by the law of large numbers $\check{\check{\boldsymbol{\Pi}}}_{\mathbf{V}}^{\perp} \xrightarrow{\text{a.s.}} \widetilde{\check{\check{\boldsymbol{\Pi}}}}_{\mathbf{V}}^{\perp}$ in the large-network limit. When \mathbf{B} is full rank, then necessarily $\boldsymbol{\Theta} = \mathbf{0}$ and the limiting

covariance matrix for Eq. (17) agrees with \mathbf{D}^{-1} . The above decomposition yields the following corollary in the form of a lemma.

Lemma A.3 (Tang et al. (2022)). *For $n \geq 1$, suppose $\mathbf{A}^{(n)} \sim \text{SBM}(\mathbf{B}, \boldsymbol{\pi})$ is a sequence of stochastic blockmodel graphs with sparsity factor ρ_n satisfying $n\rho_n = \omega(\sqrt{n})$. Provided \mathbf{B} is strictly rank deficient, then as $n \rightarrow \infty$,*

$$n\rho_n^{1/2} \text{vech}(\widehat{\mathbf{B}}^{(S)} - \widehat{\mathbf{B}}^{(L)}) - \rho_n^{-1/2} \text{vech}(\boldsymbol{\Theta}) \xrightarrow{d} \mathcal{N}(\mathbf{0}, \boldsymbol{\Gamma}). \quad (19)$$

In Eq. (19), $\boldsymbol{\Gamma} = \mathcal{L}_K(\widetilde{\boldsymbol{\Pi}}_{\mathbf{V}}^{\perp} \otimes \widetilde{\boldsymbol{\Pi}}_{\mathbf{V}}^{\perp}) \mathcal{D}_K \mathbf{D}^{-1} \mathcal{D}_K^{\top} (\widetilde{\boldsymbol{\Pi}}_{\mathbf{V}}^{\perp} \otimes \widetilde{\boldsymbol{\Pi}}_{\mathbf{V}}^{\perp})^{\top} \mathcal{L}_K^{\top}$.

The aforementioned lemmas facilitate proving the main theorems.

Proofs of Theorems 3.1 to 3.3. Recall the proposed modularity functions in Definition 3.1. Due to the associated block structure and use of $\boldsymbol{\tau}$, it holds that

$$\sum_{i,j=1}^n (A_{ij} - P_{ij}) \mathbb{I}_{\{\tau_i=\tau_j\}} = \sum_{k=1}^K n_k^2 \rho_n \left(\widehat{B}_{kk}^{(L)} - B_{kk} \right),$$

$$\sum_{i,j=1}^n (\widehat{A}_{ij} - P_{ij}) \mathbb{I}_{\{\tau_i=\tau_j\}} = \sum_{k=1}^K n_k^2 \rho_n \left(\widehat{B}_{kk}^{(S)} - B_{kk} \right),$$

and

$$\sum_{i,j=1}^n (A_{ij} - \widehat{A}_{ij}) \mathbb{I}_{\{\tau_i=\tau_j\}} = \sum_{i,j=1}^n (A_{ij} - P_{ij} - \widehat{A}_{ij} + P_{ij}) \mathbb{I}_{\{\tau_i=\tau_j\}} = \sum_{k=1}^K n_k^2 \rho_n \left(\widehat{B}_{kk}^{(L)} - \widehat{B}_{kk}^{(S)} \right).$$

Consequently, the stated asymptotic normality of Q_L , Q_S , and Q_R each hold by a direct application of Lemmas A.1 to A.3. \square

A.1.1 Comment on the influence of matrix rank

Here, we address the question raised by a referee ‘‘How robust is the asymptotic normality result for residual-based modularity if \mathbf{B} is only approximately low-rank?’’

In fact, there are some technical subtleties when dealing with Q_R for full-rank connectivity matrices \mathbf{B} . Below, we highlight why it is anticipated that the scaling of Q_R in the full-rank

setting will differ from the common scaling for Q_L and Q_S in our main theorems.

For simplicity, fix the sparsity factor $\rho_n \equiv 1$. Write $\mathbf{A} \sim \text{ER}(p)$ to indicate the adjacency matrix for a loopy undirected Erdős–Rényi random graph on n nodes with edge probability p . Note that ER graphs represent $K = 1$ stochastic blockmodel graphs that are necessarily full rank with $B_{11} = p$ and $d = 1$. Let $\widehat{\mathbf{A}}$ denote the rank-one spectral truncation of \mathbf{A} . Let $\mathbf{1}$ denote the vector of all ones, which corresponds to the ER ground-truth partition vector. For this setting, the residual variant of modularity is given by

$$\begin{aligned} Q_R &= \sum_{i,j=1}^n \left(A_{ij} - \widehat{A}_{ij} \right) \mathbb{I}_{\{\tau_i = \tau_j\}} && \text{(general definition)} \\ &= \mathbf{1}^\top (\mathbf{A} - \widehat{\mathbf{A}}) \mathbf{1}. && \text{(special form in rank one setting)} \end{aligned}$$

Write the rank-one spectral approximation of \mathbf{A} as $\widehat{\mathbf{A}} = \widehat{\lambda} \widehat{\mathbf{u}} \widehat{\mathbf{u}}^\top$ and similarly write $\mathbb{E}[\mathbf{A}] = p \mathbf{1} \mathbf{1}^\top = \lambda \mathbf{u} \mathbf{u}^\top$, where $\lambda = np$ and \mathbf{u} is the constant vector with entries $n^{-1/2}$. Let $\langle \cdot, \cdot \rangle$ denote shorthand for the Euclidean dot product. Consider the expansion of Q_R given by

$$\mathbf{1}^\top (\mathbf{A} - \widehat{\mathbf{A}}) \mathbf{1} = \langle \mathbf{A} \mathbf{1}, \mathbf{1} \rangle - \widehat{\lambda} \times |\langle \widehat{\mathbf{u}}, \mathbf{u} \rangle|^2 \times n.$$

Füredi and Komlós (1981) proved that

$$\widehat{\lambda} - np \xrightarrow{d} \mathcal{N}(1 - p, 2p(1 - p)) \quad \text{as } n \rightarrow \infty.$$

More recently, Fan et al. (2022) established that $|\langle \widehat{\mathbf{u}}, \mathbf{u} \rangle|^2$ converges in distribution to a standard normal random variable as $n \rightarrow \infty$ after appropriate centering and scaling. However, the correlation structure between $\widehat{\lambda}$ and $\widehat{\mathbf{u}}$ at the scaling of asymptotic normality is not fully understood. Furthermore, and importantly, $\langle \mathbf{A} \mathbf{1}, \mathbf{1} \rangle$ and $\widehat{\lambda}$ are strongly correlated due to the fact that \mathbf{A} is approximately a rank-one matrix. Taking all of these observations into account plausibly suggests that, under suitable conditions, $Q_R \stackrel{d}{\approx} \mathcal{N}(\mu_p, \sigma_p^2)$ for explicit expressions μ_p and σ_p^2 , and more generally provided $K = O(1)$. Preliminary simulations appear to support this conjectured behavior. Crucially, here the modularity scaling is $O(1)$, in contrast to $O(\rho_n^{-1/2} n^{-1}) = O(n^{-1})$ for the likelihood and spectral variants in the article for the dense regime $\rho_n \equiv 1$.

A.2 Extensions to more general latent space models

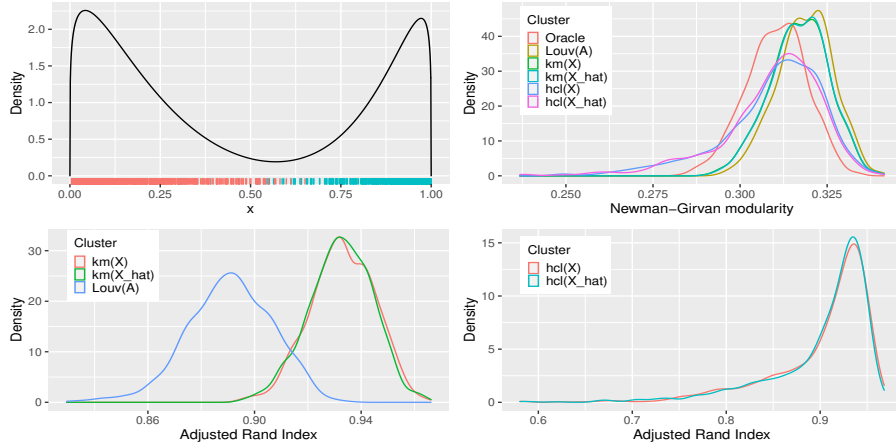


Figure 9: Mild mixture distribution setup: $t_i \sim 0.6 \times \text{Beta}(1.2, 5.5) + 0.4 \times \text{Beta}(8, 1.2)$. Clock-wise from top-left: density plot with rug plot colored as per oracle cluster of underlying distribution; Density of $Q_{\text{NG}}/2m$ for different clusters; density of ARI between clusters from hierarchical clustering (for both \mathbf{X} and $\hat{\mathbf{X}}$) and oracle; density of ARI between clusters from k -means clustering (for both \mathbf{X} and $\hat{\mathbf{X}}$) and oracle as well as Louvain clustering and oracle.

This section briefly discusses possible extensions to more expressive latent space models, namely generalized random dot product graphs (GRDPGs) from Rubin-Delanchy et al. (2022) in which edges are generated independently as

$$A_{ij} \mid \mathbf{X} \sim \text{Bernoulli} \left((\mathbf{X} \mathbf{I}_{p,q} \mathbf{X}^\top)_{ij} \right), \quad i \leq j,$$

where $p \geq 1$, $q \geq 0$ are integers such that $p + q = d$ with $\mathbf{I}_{p,q} = \mathbf{I}_p \oplus (-\mathbf{I}_q)$, and where the rows of the $n \times d$ matrix \mathbf{X} are vertex-specific so-called latent position vectors. For GRDPGs, which are capable of exhibiting richer latent space geometry than block structure, care must be taken when seeking to relate network connectivity properties with latent vector properties and the concept of network modularity. For ease of discussion, we focus on the case when $q = 0$, namely the consideration of so-called random dot product graphs (RDPGs).

Stochastic blockmodels are special cases of GRDPGs, and similarly, SBMs with positive semidefinite connectivity matrices are special cases of RDPGs. In particular, in a K -block SBM, the rows of the latent position matrix \mathbf{X} each take one of K distinct values based on the block membership of the corresponding node. In this case, the community membership vector $\boldsymbol{\tau}$ is either predefined with

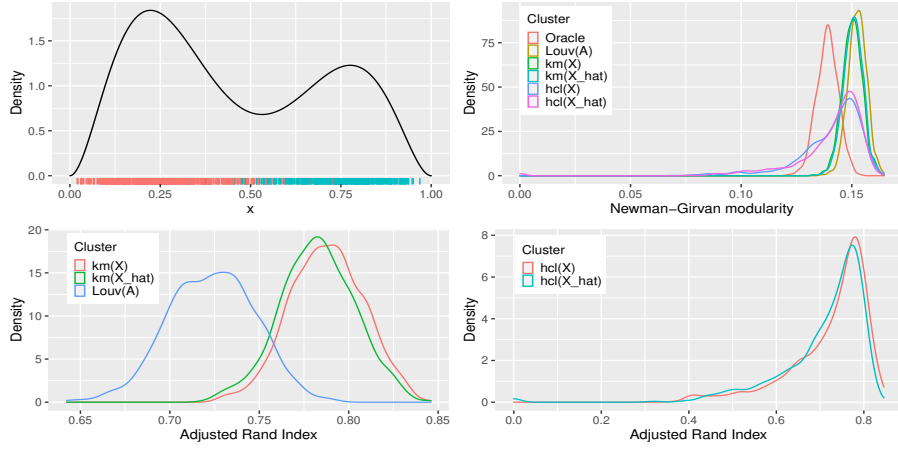


Figure 10: Moderate mixture distribution setup: $t_i \sim 0.6 \times \text{Beta}(3, 8) + 0.4 \times \text{Beta}(8, 3)$. Clock-wise from top-left: density plot with rug plot colored as per oracle cluster of underlying distribution; Density of $Q_{\text{NG}}/2m$ for different clusters; density of ARI between clusters from hierarchical clustering (for both \mathbf{X} and $\hat{\mathbf{X}}$) and oracle; density of ARI between clusters from k -means clustering (for both \mathbf{X} and $\hat{\mathbf{X}}$) and oracle as well as Louvain clustering and oracle.

$\tau_i = \tau_j$ if and only if $\mathbf{X}_i = \mathbf{X}_j$, namely the i -th and j -th row vectors of \mathbf{X} are equal. In general, an explicit concept or definition of community membership is needed in order to define a modularity value. One possible approach for RDPGs is to assign $\tau_i = \tau_j$ if and only if $d(\mathbf{X}_i, \mathbf{X}_j) \leq \epsilon$ for some specified distance metric $d(\cdot, \cdot)$ and user-selected tolerance $\epsilon > 0$.

The example provided here is inspired by the treatment in [Athreya et al. \(2021\)](#). First, generate i.i.d. random variables $t_i \sim p \times \text{Beta}(a_1, b_1) + (1 - p) \times \text{Beta}(a_2, b_2)$, where $0 < p < 1$. Second, determine the latent position vectors via the function $\mathbf{x}(t) := [t^2, 2t(1 - t), (1 - t)^2]$, yielding points (vectors) on the so-called one-dimensional Hardy–Weinberg curve in the unit simplex. Given $i \in \llbracket n \rrbracket$, the latent positions $\mathbf{x}(t_i)$ are aggregated row-wise to form the matrix \mathbf{X} . In this example, an “oracle” cluster membership is available via the coefficients of the mixture distribution. We choose $d(\mathbf{x}, \mathbf{y}) := \|\mathbf{x} - \mathbf{y}\|_{\ell_2}$ and opt to hard-cluster the latent positions as our proxy for ground truth. In general, supposing the underlying mixture were composed of K distributions, one could choose the number of true clusters to be larger or smaller than K depending on the separability of the component distributions.

We consider two modeling situations. In Fig. 9, $t_i \sim 0.6 \times \text{Beta}(1.2, 5.5) + 0.4 \times \text{Beta}(8, 1.2)$ exhibits mild overlap between the component distributions. In Fig. 10, $t_i \sim 0.6 \times \text{Beta}(3, 8) + 0.4 \times \text{Beta}(8, 3)$ exhibits moderate overlap between the component distributions. The networks generated

subsequently have $n = 2000$ vertices and are independently simulated 1000 times. Hierarchical clustering with average linkage on \mathbf{X} is chosen to partition the nodes into two communities. For comparison, the same technique is applied to $\widehat{\mathbf{X}}$, the adjacency spectral embedding of \mathbf{A} . We also use the k -means algorithm on both \mathbf{X} and $\widehat{\mathbf{X}}$ since the hard clustering technique employs the ℓ_2 distance. Further, we apply the Louvain algorithm as a choice for community detection that directly takes the networks as input. In the two figures, we show the underlying mixture distributions, the Newman–Girvan modularity for the different sources of clusters, $Q_{\text{NG}}/2m$, and the ARI between the oracle clusters and each of the different true and estimated clusterings. The ARI plots show that in the mild mixture setup, estimated clustering with $\widehat{\mathbf{X}}$ captures the corresponding true clustering with high accuracy. In contrast, for the moderate mixture, deteriorated performance is observed. Louvain clustering performs much worse in recovering the oracle in both examples. The density plots for $Q_{\text{NG}}/2m$ repeatedly exhibit relatively large modularity values in the mild mixture case for all sources of clusters.

The Newman–Girvan modularity, Q_{NG} , is the most commonly used modularity function for partitioning networks. The underlying null network depends only on the degree distribution of the observed graph. For one-dimensional RDPGs, consider $\mathbf{X} = [k_1/\sqrt{2m}, k_2/\sqrt{2m}, \dots, k_n/\sqrt{2m}]^\top$. In such cases, clustering based on \mathbf{X} will resemble clustering based on node-degrees. In certain cases, the Newman–Girvan modularity shows relatively poor performance in detecting node-clusters and fails in some other situations as shown in Section 4. One might instead select Q_{L} as a choice for modularity if the edge generating distribution is plausibly Bernoulli. If, as for SBMs, the adjacency matrix \mathbf{A} is generated using a block probability matrix \mathbf{B} where the underlying community structure is unknown, then the $(A_{ij} - B_{\tau_i\tau_j})$ can be interpreted as mean zero noise. If the objective is to detect clusters via noise or residual minimization, one may consider the least squares approach in [Lei et al. \(2019\)](#).

A.3 Power analysis

This section provides a brief illustration pertaining to the discussion in Section 3.3. Consider $\mathbf{B}^{(0)} = \mathbf{v}\mathbf{v}^\top$ and $\mathbf{B}^{(1)} = \mathbf{u}\mathbf{u}^\top$ where $u_1 = v_1 + \epsilon$, $u_2 = v_2$. Setting $\mathbf{v} = [3/4, 1/4]^\top$, $\boldsymbol{\pi} = [1/4, 3/4]^\top$ and $\rho_n \equiv 1$, we generate $\mathbf{A} \sim \text{SBM}(\mathbf{B}^{(1)}, \boldsymbol{\pi})$ for $n \in \{100, 500, 1000\}$ and $\epsilon \in \{0.02, 0.05\}$. We report the empirical performance across 1000 independent simulation trials. Table 3 presents

results for $\epsilon = 0.02$, while Table 4 presents results for $\epsilon = 0.05$. Both are as expected. Here, the connectivity matrix under the null is

$$\mathbf{B}^{(0)} = \begin{bmatrix} 0.5625 & 0.1875 \\ 0.1875 & 0.0625 \end{bmatrix},$$

whereas the choices $\epsilon = 0.02$ and 0.05 yield alternatives

$$\mathbf{B}^{(1)} = \begin{bmatrix} 0.5929 & 0.1925 \\ 0.1925 & 0.0625 \end{bmatrix} \text{ and } \begin{bmatrix} 0.6400 & 0.2000 \\ 0.2000 & 0.0625 \end{bmatrix}, \text{ respectively.}$$

n	Power for T_L			Power for T_S		
	Analytic	Empirical	Emp. with plug-in	Analytic	Empirical	Emp. with plug-in
100	0.093	0.099	0.094	0.1284	0.152	0.147
500	0.8641	0.855	0.856	0.9772	0.938	0.938
1000	0.99998	1	1	1	1	1

Table 3: Power analysis for T_L and T_S when $\epsilon = 0.02$.

n	Power for T_L			Power for T_S		
	Analytic	Empirical	Emp. with plug-in	Analytic	Empirical	Emp. with plug-in
100	0.3424	0.357	0.365	0.5426	0.549	0.555
500	1	1	1	1	1	1
1000	1	1	1	1	1	1

Table 4: Power analysis for T_L and T_S when $\epsilon = 0.05$.

A.4 Example 4: graphs with $K = 3$, $d = 1$, balanced, core-periphery

Consider a three-block SBM where \mathbf{B} takes the form $\begin{bmatrix} p \\ p^2 \\ p^3 \end{bmatrix} \times [p \ p^2 \ p^3]$. Set

$$p = 3/4, \quad \mathbf{B} = \begin{bmatrix} 0.5625000 & 0.4218750 & 0.3164062 \\ 0.4218750 & 0.3164062 & 0.2373047 \\ 0.3164062 & 0.2373047 & 0.1779785 \end{bmatrix}, \quad \boldsymbol{\pi} = \begin{bmatrix} 1/3 \\ 1/3 \\ 1/3 \end{bmatrix}, \quad n \in \{300, 600, 1200, 1800\}.$$

We again simulate 1000 independent trials. The results for residual-based modularity are presented in Fig. 11. The Louvain algorithm shows similar performance as in the earlier example; ARI is almost always near zero, and the number of clusters is dramatically overestimated.

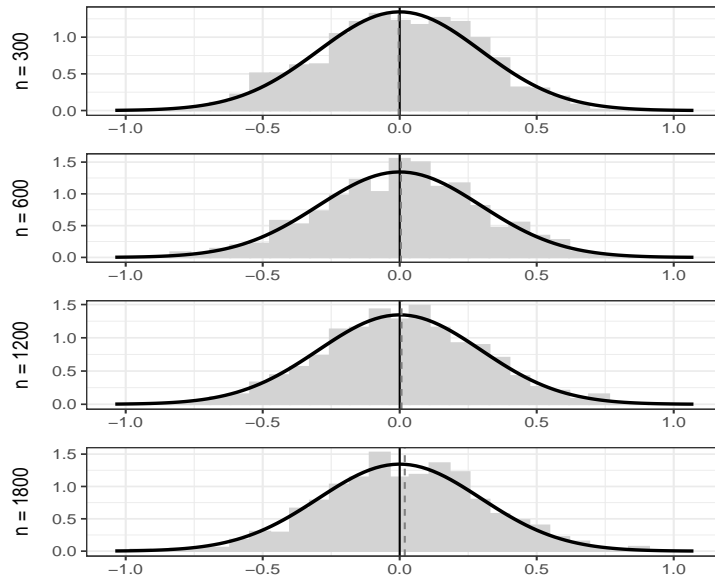


Figure 11: Dense networks and residual-based modularity in Appendix A.4. Dashed vertical line shows bias in simulation. Solid vertical line shows population bias. Solid curve shows population density fit.

A.5 Further examples illustrating modularity asymptotics

Section 4 illustrates theoretical properties of the modularity functions via simulation. In Section 4.0.3 and Appendix A.4 which consider rank-degenerate \mathbf{B} matrices, the residual-based modularity function is investigated. For completeness, here we show the performance of Q_L and Q_S in each of these settings. Further, for the setup in Section 4.0.3 we now present the $\rho_n \equiv 1$ setting in Fig. 12. The empirical values of the parameters closely agree with the asymptotic, analytic population values. Here, too, the performance of the Louvain algorithm is predictably poor, with adjusted Rand index values near zero and estimated number of clusters much larger than the ground truth value, since the underlying block probability matrix has core-periphery structure.

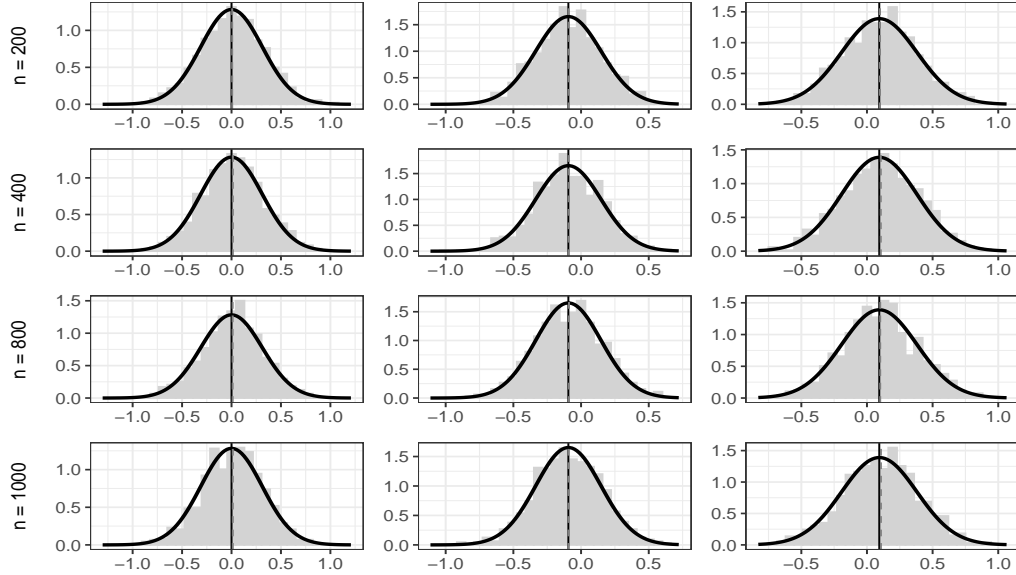


Figure 12: Dense case simulations for Section 4.0.3. Left to right panels are for $\rho_n^{-1/2} n^{-1} Q_L$, $\rho_n^{-1/2} n^{-1} Q_S$, and $\rho_n^{-1/2} n^{-1} Q_R$, respectively. Dashed vertical line shows bias in simulation. Solid vertical line shows population bias. Solid curve shows population density fit.

A.6 COBRE data: additional discussion

The Power parcellation consists of fourteen brain systems: 1. *Sensory/somatomotor Hand* (30 nodes), 2. *Sensory/somatomotor Mouth* (5 nodes), 3. *Cingulo-opercular Task Control* (14 nodes), 4. *Auditory* (13 nodes), 5. *Default mode* (58 nodes), 6. *Memory retrieval* (5 nodes), 7. *Visual* (31 nodes), 8. *Fronto-parietal Task Control* (25 nodes), 9. *Saliency* (18 nodes), 10. *Subcortical* (13 nodes), 11. *Ventral attention* (9 nodes), 12. *Dorsal attention* (11 nodes), 13. *Cerebellar* (4 nodes), and 14. *Uncertain* (28 nodes). On the basis of function, we also consider a coarser partition into $\hat{K} = 5$ communities, specifically of the form $\{\{1, 2, 3, 4\}, \{5, 6, 8, 9\}, \{7, 12\}, \{10, 11, 13\}, \{14\}\}$.

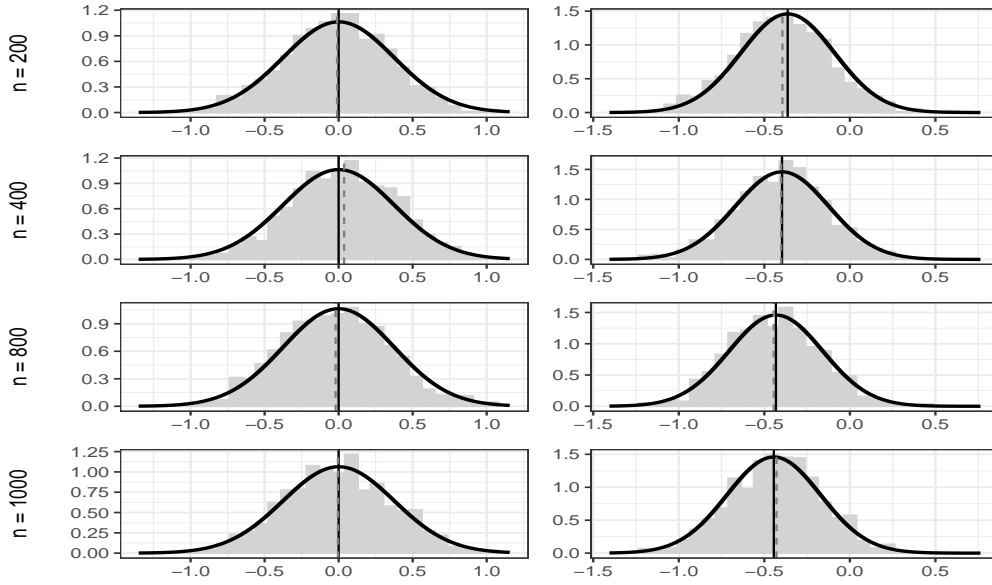


Figure 13: Sparse case simulations for Section 4.0.3. Left panel is $\rho_n^{-1/2} n^{-1} Q_L$ and right panel is $\rho_n^{-1/2} n^{-1} Q_S$. Dashed vertical line shows bias in simulation. Solid vertical line shows population bias. Solid curve shows population density fit.

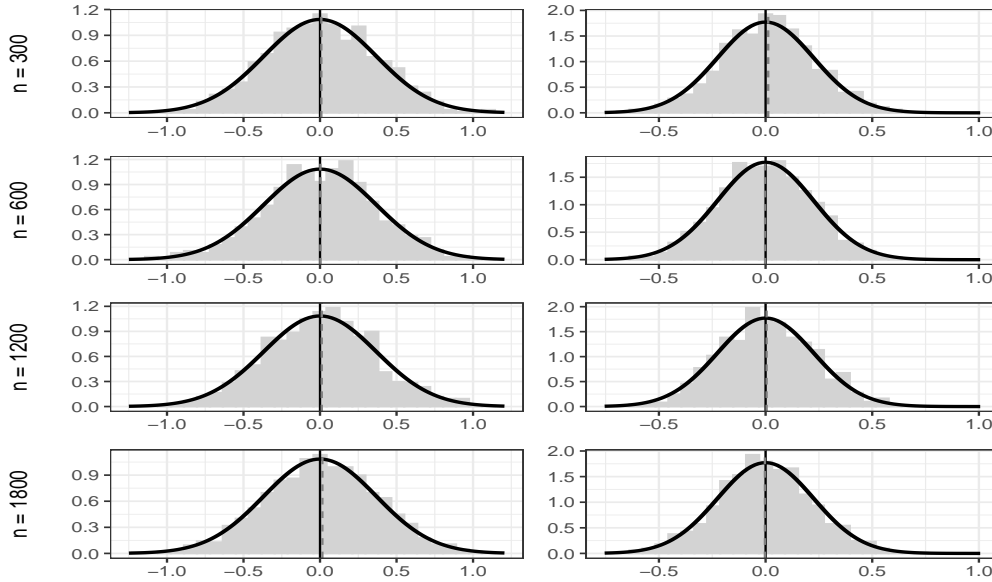


Figure 14: Additional simulations for Appendix A.4. Left and right panels are for $\rho_n^{-1/2} n^{-1} Q_L$ and $\rho_n^{-1/2} n^{-1} Q_S$, respectively. Dashed vertical line shows bias in simulation. Solid vertical line shows population bias. Solid curve shows population density fit.